

Neuronal Excitability

The Maintenance of Synaptic Homeostasis at the *Drosophila* Neuromuscular Junction Is Reversible and Sensitive to High Temperature

Catherine J. Yeates,^{1,2} Danielle J. Zwiefelhofer,¹ and C. Andrew Frank^{1,3}DOI:<http://dx.doi.org/10.1523/ENEURO.0220-17.2017>

¹Department of Anatomy and Cell Biology, University of Iowa Carver College of Medicine, Iowa City, IA 52242, ²Interdisciplinary Graduate Program in Neuroscience, University of Iowa, Iowa City, IA 52242, and ³Interdisciplinary Programs in Neuroscience, Genetics, and Molecular Medicine, University of Iowa, Iowa City, IA 52242

Abstract

Homeostasis is a vital mode of biological self-regulation. The hallmarks of homeostasis for any biological system are a baseline set point of physiological activity, detection of unacceptable deviations from the set point, and effective corrective measures to counteract deviations. Homeostatic synaptic plasticity (HSP) is a form of neuroplasticity in which neurons and circuits resist environmental perturbations and stabilize levels of activity. One assumption is that if a perturbation triggers homeostatic corrective changes in neuronal properties, those corrective measures should be reversed upon removal of the perturbation. We test the reversibility and limits of HSP at the well-studied *Drosophila melanogaster* neuromuscular junction (NMJ). At the *Drosophila* NMJ, impairment of glutamate receptors causes a decrease in quantal size, which is offset by a corrective, homeostatic increase in the number of vesicles released per evoked presynaptic stimulus, or quantal content. This process has been termed presynaptic homeostatic potentiation (PHP). Taking advantage of the GAL4/GAL80^{TS}/UAS expression system, we triggered PHP by expressing a dominant-negative glutamate receptor subunit at the NMJ. We then reversed PHP by halting expression of the dominant-negative receptor. Our data show that PHP is fully reversible over a time course of 48–72 h after the dominant-negative glutamate receptor stops being genetically expressed. As an extension of these experiments, we find that when glutamate receptors are impaired, neither PHP nor NMJ growth is reliably sustained at high culturing temperatures (30–32°C). These data suggest that a limitation of homeostatic signaling at high temperatures could stem from the synapse facing a combination of challenges simultaneously.

Key words: *Drosophila*; homeostatic; neuromuscular; plasticity; reversibility; synapse

Significance Statement

Biological homeostatic systems must upregulate or downregulate cellular parameters to maintain appropriate set points of physiologic activity. Homeostasis is a well-documented mode of regulation in metazoan nervous systems. True homeostatic control should be a reversible process. Because of technical difficulties of presenting and removing functional challenges to living synapses, the reversibility of homeostatic forms of synapse regulation has not been rigorously examined *in vivo* over extended developmental time. Here we formally demonstrate that a form of long-term homeostatic regulation of *Drosophila melanogaster* neuromuscular synapse function is reversible and temperature labile. This is significant because developing methods to study how homeostatic regulatory systems are turned on and off could lead to fundamental new insights about control of synaptic output.

Introduction

Homeostasis is a strong form of biological regulation. It permits individual cells or entire systems of cells to maintain core physiologic properties that are compatible with life. In the nervous system, decades of study have shown that while synapses and circuits are inherently plastic, they also possess robust homeostatic regulatory systems to maintain physiologic stability. Homeostatic plasticity in the nervous system is a non-Hebbian strategy to counteract challenges to neuronal function that may threaten to disrupt essential neuronal and circuit activities (Turrigiano, 2017). Depending on the synaptic preparation examined and the environmental challenge presented to the synapse, homeostatic responses may be executed via compensatory adjustments to presynaptic neurotransmitter release (Cull-Candy et al. 1980; Petersen et al. 1997; Murthy et al. 2001; Thiagarajan et al. 2005; Frank et al. 2006; Davis and Müller, 2015), postsynaptic neurotransmitter receptor composition (O'Brien et al. 1998; Turrigiano et al. 1998; Rongo and Kaplan, 1999; Turrigiano, 2008), neuronal excitability (Marder and Prinz, 2002; Marder and Goaillard, 2006; Marder and Bucher, 2007; Bergquist et al. 2010; Parrish et al. 2014), or even developmentally, via changes in synaptic contact formation and maintenance (Davis and Goodman, 1998; Burrone et al. 2002; Wefelmeyer et al. 2016).

Bidirectionality has been documented in several homeostatic systems, perhaps most prominently in the case of synaptic scaling of neurotransmitter receptors. For vertebrate neuronal culture preparations—such as cortical neurons or spinal neurons—global silencing of network firing can induce increases in excitatory properties, such as increased AMPA-type glutamate receptor accumulation; by contrast, global enhancement of activity can induce the opposite type of response (O'Brien et al. 1998; Turrigiano et al. 1998; Wierenga et al. 2005; Turrigiano, 2008). Bidirectionality is also a key feature underlying homeostatic alterations of neurotransmitter release at pe-

ripheral synapses such as the neuromuscular junction (NMJ). At the NMJs of *Drosophila melanogaster* and mammals, impairing neurotransmitter receptor function postsynaptically results in diminished sensitivity to single vesicles of transmitter. Electrophysiologically, this manifests as decreased quantal size. NMJs respond to this challenge by enhancing neurotransmitter vesicle release (Cull-Candy et al. 1980; Plomp et al. 1992, 1995; Petersen et al. 1997; Davis et al. 1998; Frank et al. 2009). By contrast, perturbations that enhance quantal size—for example, overexpression of a vesicular neurotransmitter transporter in *Drosophila*—can result in decreased quantal content (Daniels et al. 2004; Gaviño et al. 2015).

Synapses and circuits possess myriad solutions to assume appropriate functional outputs in the face of perturbations (Marder and Prinz, 2002; Marder and Goaillard, 2006). Therefore, a corollary to bidirectional regulation is that homeostatic forms of regulation should also be reversible. There are experimental difficulties of presenting and removing a synaptic challenge in the context of a living synapse, so homeostatic reversibility has not been rigorously studied in an *in vivo* system or over extended periods of developmental time. Understanding how homeostatic regulatory systems are reversibly turned on and off could have profound implications for elucidating fundamental properties of circuit regulation.

Here we exploit the *Drosophila* NMJ as a living synapse to test homeostatic reversibility. At the *Drosophila* NMJ, a canonical way to challenge synapse function is through glutamate receptor impairment (Frank, 2014), either genetically (Petersen et al. 1997) or pharmacologically (Frank et al. 2006). Impairments of muscle glutamate receptor function decrease quantal size. Decreased quantal size spurs muscle-to-nerve signaling that ultimately results in a homeostatic increase in presynaptic vesicle release, a process that has been termed presynaptic homeostatic potentiation (PHP). The most widely used experimental homeostatic challenges to *Drosophila* NMJ function are not easily reversed. These challenges include genetic deletion of the glutamate receptor subunit GluRIIA (Petersen et al. 1997) and the mostly irreversible pharmacological inhibition of glutamate receptors with Philanthotoxin-433 (PhTox; Frank et al. 2006).

For this study, we engineered a way to challenge NMJ function *in vivo* for significant periods of time, verify the effectiveness of the challenge at a defined developmental time point, remove the challenge, and then assess the homeostatic capacity of the NMJ at a later developmental time point. By using the temporal and regional gene expression targeting (TARGET) GAL4/GAL80^{TS}/UAS expression system (McGuire et al. 2003) to temporally control the expression of a dominant-negative GluRIIA receptor subunit (DiAntonio et al. 1999), we found that homeostatic potentiation of neurotransmitter release is fully reversible. In the course of conducting our studies, we also uncovered a high temperature limitation of homeostatic potentiation at the NMJ.

Received June 25, 2017; accepted November 23, 2017; First published December 04, 2017.

The authors declare no competing financial interests.

Author contributions: C.J.Y. and C.A.F. designed research; C.J.Y. and D.J.Z. performed research; C.J.Y., D.J.Z., and C.A.F. analyzed data; C.J.Y. and C.A.F. wrote the paper drafts, with editing done by C.J.Y., D.J.Z., and C.A.F.

Funding supporting this work includes a Whitehall Foundation Grant (2014-08-03), an NSF Grant (1557792), and an NIH/NINDS Grant (R01NS085164) to C.A.F. C.J.Y. was supported in part by an NIH/NINDS Predoctoral Training Grant to the University of Iowa (UI) Interdisciplinary Graduate Program in Neuroscience (T32NS007421 – PI Daniel T. Tranel), as well as a Post-comprehensive exam Predoctoral Summer fellowship and a Ballard and Seashore Dissertation fellowship via the Graduate College at UI.

Acknowledgments: We thank members of the Frank, Tootle, Lin, Kitamoto, Wallrath, and Geyer labs for helpful discussions.

Correspondence should be addressed to C. Andrew Frank, Ph.D., Department of Anatomy and Cell Biology, University of Iowa Carver College of Medicine, 51 Newton Rd, 1-661A BSB, Iowa City, IA 52242. E-mail: andy-frank@uiowa.edu.

DOI: <http://dx.doi.org/10.1523/ENEURO.0220-17.2017>

Copyright © 2017 Yeates et al.

This is an open-access article distributed under the terms of the Creative Commons Attribution 4.0 International license, which permits unrestricted use, distribution and reproduction in any medium provided that the original work is properly attributed.

Materials and Methods

Drosophila stocks and husbandry

Fruit fly stocks were obtained from either the Bloomington *Drosophila* Stock Center (BDSC) or the labs that generated them. w^{1118} was used as a wild-type (WT) control (Hazelrigg et al. 1984). The *GluRIIA*^{SP16} deletion was used as a genetic loss-of-function (Petersen et al. 1997). Transgenes included the UAS-driven dominant-negative glutamate receptor subunit, *UAS-GluRIIA*^{M614R} (DiAntonio et al. 1999), and a ubiquitous *Tubulin*_{Promoter}-*Gal80*^{TS} (*Tub_P-Gal80*^{TS}; McGuire et al. 2003). Muscle-specific GAL4 drivers included *MHC-Gal4* (Schuster et al. 1996a, b) and *BG57-Gal4* (also commonly known as *C57-Gal4*; Budnik et al. 1996). For reversibility experiments, the full genotypes for the crosses were $w^{1118}; CyO-GFP/UAS-GluRIIA$ ^{M614R}; *TM6b(Tb)/Tub_P-Gal80*^{TS} males × $w^{1118}; TM6b(Tb)/MHC-Gal4$ or *BG57-Gal4* virgin females. Non-tubby, non-GFP larvae were selected for recording. In control recordings, we found no discernable differences between male and female third-instar electrophysiology, but for reversibility experiments (Figs. 4–6), single sexes of larvae were chosen to eliminate sex as a possible confounding variable.

Fruit flies were raised on cornmeal, molasses, and yeast medium (see BDSC website for standard recipe) in temperature-controlled conditions. For most experiments, animals were reared at the temperatures noted (including temperature shifts) until they reached the wandering third instar larval stage, at which point they were chosen for electrophysiological recording. For experiments in Figs. 3 and 4, mated animals were placed at either 21°C, 25°C, or 29°C and allowed to lay eggs for 6–8 h. Stage- and size-matched early third instar larvae (~48–54 h after egg laying) were subjected to electrophysiological recording (Fig. 3) or temperature swaps (Figs. 4–6), as indicated.

Electrophysiology and analysis

For Figs. 1, 2, and 4–7, wandering third instar larvae were filleted for electrophysiological recordings. For Fig. 3, early third instar larvae were used. In both cases, sharp electrode electrophysiological recordings were taken from muscle 6 of abdominal segments 2 and 3. Briefly, larvae were dissected in a modified HL3 saline comprising NaCl (70 mM), KCl (5 mM), MgCl₂ (10 mM), NaHCO₃ (10 mM), sucrose (115 mM = 3.9%), trehalose (4.2 mM = 0.16%), Hepes (5.0 mM = 0.12%), and CaCl₂ (0.5 mM). Electrophysiological data were collected using an Axopatch 200B amplifier (Molecular Devices) in bridge mode, digitized using a Digidata 1440A data acquisition system (Molecular Devices), and recorded with pCLAMP 10 acquisition software (Molecular Devices). Spontaneous miniature excitatory postsynaptic potential (mEPSP) data were acquired at a sampling rate of 10,000 Hz (one sample/100 μs). The low-pass and high-pass settings were 5 kHz and 1 Hz, respectively. A Master-8 pulse stimulator (A.M.P. Instruments) and an ISO-Flex isolation unit (A.M.P. Instruments) were used to deliver 1-ms suprathreshold stimuli to the appropriate segmental nerve. The average mEPSP amplitude per NMJ was quantified (MiniAnalysis, Synaptosoft), ~100–200 individual spontaneous release

events per NMJ. The noise level for each individual mEPSP event was captured in the same analysis. From this number (noise could be positive or negative when captured by the software), a positive *Inoise1* value was assigned to each mEPSP and averaged across all mEPSPs for a given NMJ. This allowed calculation of both mEPSP noise and mEPSP signal:noise ratios (Table 1). In the case that the mEPSP frequency was extremely low (usually for expression of the dominant-negative glutamate receptor subunit), several minutes of spontaneous recording were done, and all events were measured. Measurements from all NMJs of a given condition were then averaged. For evoked neurotransmission, 30 excitatory postsynaptic potentials (EPSPs) were averaged to find a value for each NMJ. These were then averaged to calculate a value for each condition. Quantal content (QC) was calculated by the ratio of average EPSP and average mEPSP amplitudes for each individual NMJ. An average QC was then calculated for each condition.

NMJ immunostaining

Wandering third instar larvae were selected and filleted. Dissected animals were fixed for 4 min in Bouin's fixative (Ricca Chemical Company), washed using standard procedures, and incubated in primary antibodies at room temperature for 2 h. This was followed by additional washes and another 2-h incubation in secondary antibody at room temperature. Bouton staining was performed to assess NMJ growth by using the following primary antibodies: mouse anti-Synapsin (anti-Syn; 3C11) 1:50 (Developmental Studies Hybridoma Bank) and rabbit anti-Dlg 1:15,000 (Budnik et al. 1996). The following fluorophore-conjugated secondary antibodies were also used (Jackson ImmunoResearch Laboratories): goat anti-mouse 488 1:1000 (DyLight) and goat anti-rabbit 549 1:2000 (DyLight). Larval preparations were mounted in Vectashield (Vector Laboratories) and imaged at room temperature using Zen software on a Zeiss 700 LSM mounted on an Axio Observer.Z1 with an EC Plan-Neofluar 40× Oil DIC Objective (aperture 1.30) or an EC Plan-Apochromat 63× Oil DIC Objective (aperture 1.40; Zeiss). Experimental and control larval preps were imaged using identical acquisition settings, and analyzed using the same procedure and thresholds. Images were prepared for publication in Adobe Photoshop using identical procedures for experimental and control images. Anti-Dlg bouton counts were done by hand in a blinded fashion to quantify synapse growth. For each anti-Dlg-positive bouton counted in muscle, it was verified that there was a corresponding cluster of anti-Syn staining in neurons.

Statistical analyses

Statistical analyses were conducted using GraphPad Prism software. For normally distributed data, statistical significance was assessed by either Student's *t* test, when one experimental data set was being directly compared to a control data set, or one-way ANOVA with Tukey's *post hoc* test when multiple data sets were being compared. Specific *p* value ranges are noted in the figure legends and shown in graphs as **p* < 0.05; ***p* < 0.01; and ****p* < 0.001. For some comparisons that potentially trend toward *p* < 0.05 statistical significance but do not

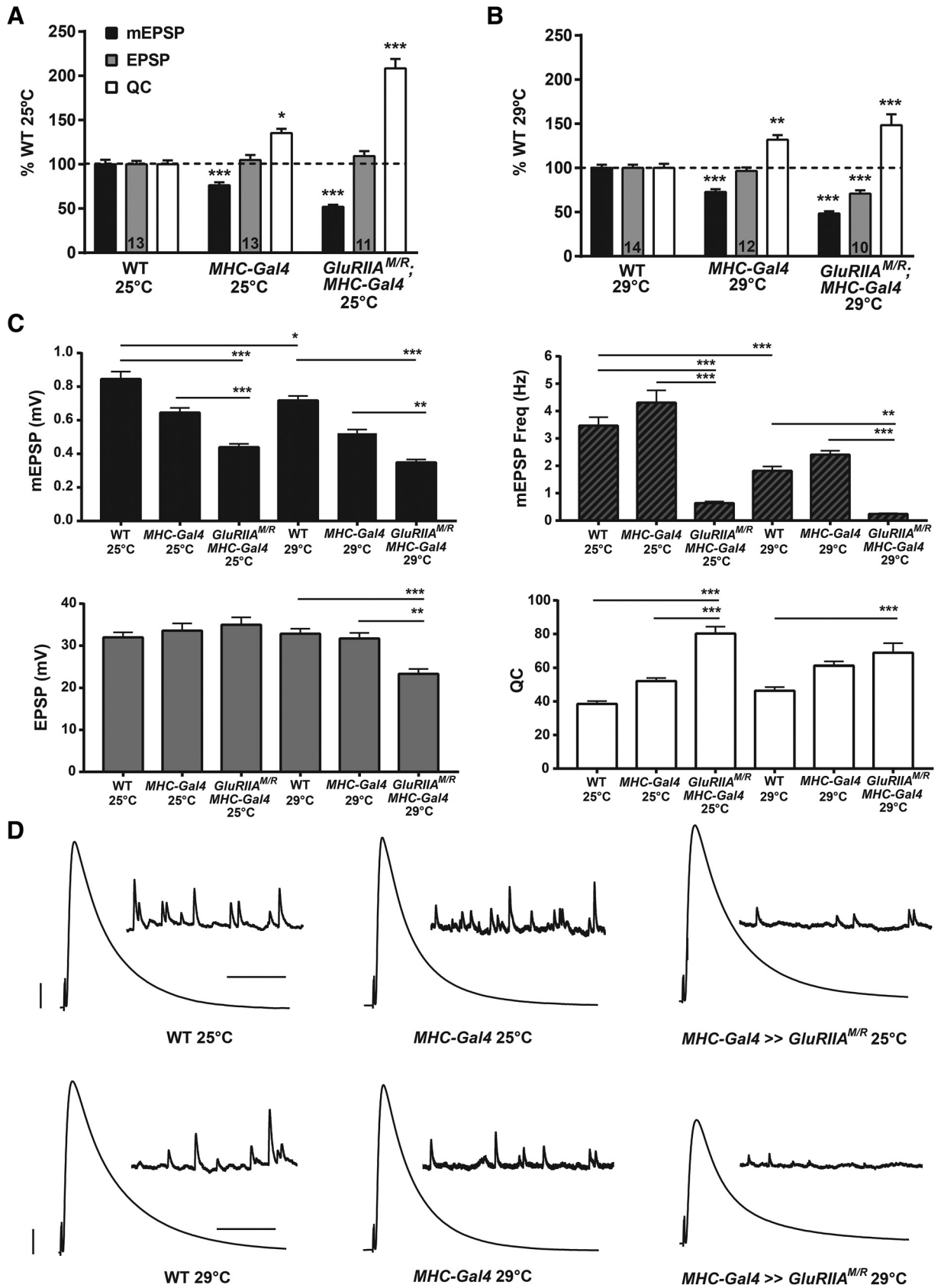


Figure 1. Postsynaptic expression of GluRIIA^{M/R} causes a decrease in mEPSP size and a homeostatic increase in quantal content. **A**, Electrophysiological profiles comparing WT (*w¹¹¹⁸*) NMJs to NMJs expressing driver alone (*w¹¹¹⁸; MHC-Gal4/+*) and NMJs with

continued

postsynaptic expression of a dominant-negative transgene *UAS-GluRIIA^{M/R}* (*w; UAS-GluRIIA^{M/R}/+; MHC-Gal4/+*). Animals were reared at 25°C. Driver controls showed a significant decrease in mEPSP amplitude ($***p < 0.001$) and increase in quantal content ($*p < 0.05$) compared to WT. mEPSP amplitude in the dominant-negative was even more markedly decreased compared to WT ($***p < 0.001$). Quantal content (QC) was significantly increased for the dominant-negative NMJs ($***p < 0.001$), revealing a homeostatic system that maintains EPSP amplitude at control levels. **B**, The same genotypes as in **A**, raised at 29°C. Driver controls showed a baseline decrease in mEPSP amplitude ($***p < 0.001$) and an increase in quantal content ($***p < 0.01$). mEPSP amplitude was significantly decreased in the dominant-negative ($***p < 0.001$) compared to WT. EPSP amplitude was also decreased in the dominant-negative compared to WT ($***p < 0.001$), with QC significantly increased ($***p < 0.001$) but not enough to completely offset the decrease in quantal size. **C**, Raw value comparisons of the recordings normalized in **A** and **B**. mEPSP amplitude, mEPSP frequency, EPSP amplitude, and QC were compared for all six conditions. In addition to the observations above, WT at 29°C had decreased mEPSP amplitude ($*p < 0.05$) and mEPSP frequency ($***p < 0.001$) compared to WT at 25°C. There was no difference in quantal content between the two WT conditions ($p = 0.38$). mEPSP amplitude was decreased in the dominant-negatives compared to driver controls at 25°C ($***p < 0.001$) and 29°C ($**p < 0.01$). At 25°C, the dominant-negative showed a marked decrease in mEPSP frequency compared to WT at the same temperature ($***p < 0.001$). The dominant-negative at 29°C also showed a significant decrease in mEPSP frequency compared to WT at 29°C ($**p < 0.01$). Dominant-negative animals also showed significant decreases in mEPSP frequency compared to driver controls at their respective temperatures ($***p < 0.001$). QC was significantly increased in dominant-negative animals compared to driver controls at 25°C ($***p < 0.001$). **D**, Electrophysiological traces. Scale bars for EPSPs (and mEPSPs) are 5 mV (1 mV) and 50 ms (1000 ms). All statistical comparisons done by one-way ANOVA with Tukey's *post hoc*, collectively comparing the six total conditions.

achieve it ($0.05 < p < 0.1$), specific values are reported on the graph itself. mEPSP size frequency distributions were analyzed by Kruskal-Wallis test (Fig. 2, comparing three conditions) and Mann-Whitney test (Fig. 3, comparing two conditions) and plotted as cumulative histograms and as box-and-whisker plots. To assess correlations between incubation temperature recovery times and electrophysiological parameters (Fig. 5), nonlinear best-fit curves were generated using quadratic equations. These curves were graphed on top of the raw data, with R^2 values for the curves reported in the Fig. 5 legend. Most values reported in Table 1 or plotted on bar graphs are mean \pm SEM. For box-and-whisker plots, cumulative data are plotted in a box denoting 25th–75th percentiles (bar denotes medi-

logical parameters (Fig. 5), nonlinear best-fit curves were generated using quadratic equations. These curves were graphed on top of the raw data, with R^2 values for the curves reported in the Fig. 5 legend. Most values reported in Table 1 or plotted on bar graphs are mean \pm SEM. For box-and-whisker plots, cumulative data are plotted in a box denoting 25th–75th percentiles (bar denotes medi-

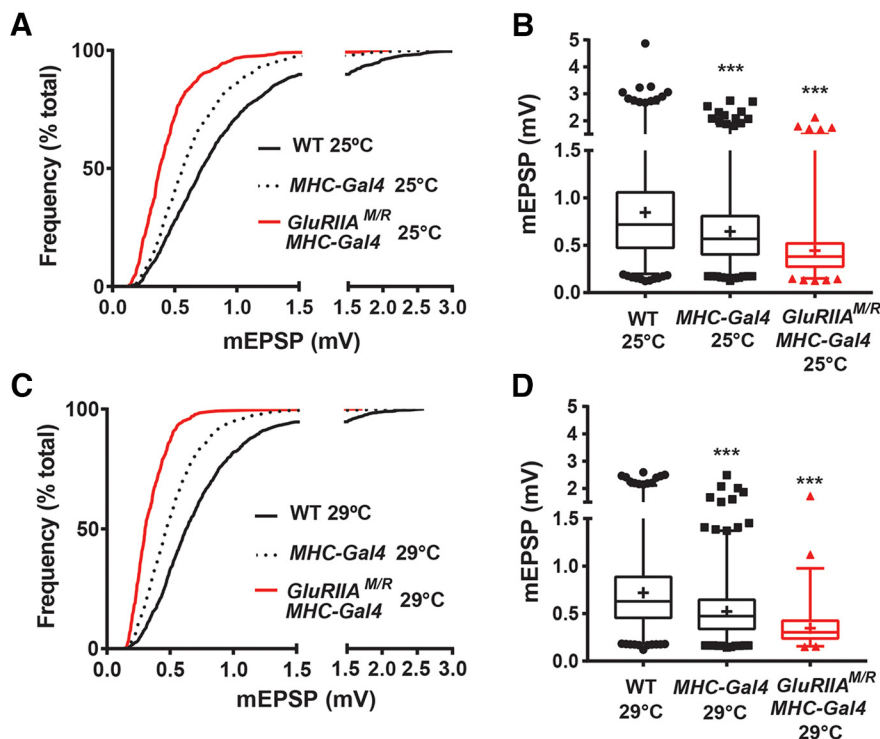


Figure 2. mEPSP amplitude distribution is leftward-shifted for muscle GAL4 driver controls and dominant-negative NMJs. **A**, Cumulative frequency distributions plotting mEPSP values for WT, *w; MHC-Gal4/+*, and *w; UAS-GluRIIA^{M/R}/+; MHC-GAL4/+* NMJs at 25°C. **B**, Box-and-whisker plots of mEPSP amplitude for the same genotypes. Driver controls and dominant-negatives both showed significantly diminished mEPSP distribution profiles compared to WT ($***p < 0.001$, Kruskal-Wallis test). **C**, Cumulative frequency distribution comparing mEPSP values for WT, *w; MHC-Gal4/+*, and *w; UAS-GluRIIA^{M/R}/+; MHC-GAL4/+* at 29°C. **D**, Box-and-whisker plots of mEPSP amplitude for the same genotypes. Driver controls and dominant-negatives both show significantly diminished mEPSP distribution profiles compared to WT ($***p < 0.001$, Kruskal-Wallis test).

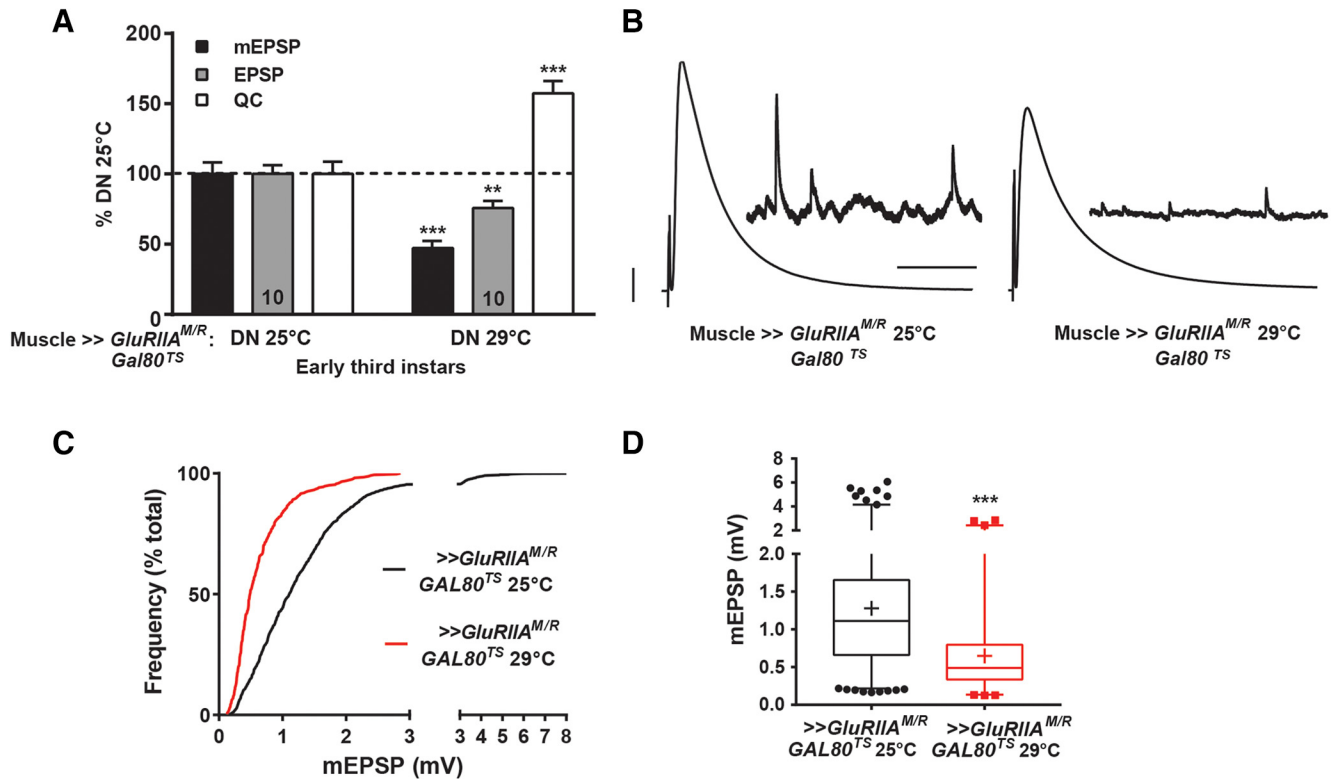


Figure 3. Animals expressing *GluRIIA^{M/R}* show homeostatic compensation early in development. **A**, *w*; *GluRIIA^{M/R}/+*; *MHC-GAL4/GAL80^{TS}* animals were reared at 25°C or 29°C, and recordings were performed on early third instar larvae. The animals reared at 29°C had a marked decrease in average mEPSP amplitude compared to animals reared at 25°C (****p* < 0.001, Student’s *t* test), as well as a decrease in mEPSP frequency (*p* < 0.001, see Table 1). EPSP amplitude was decreased at 29°C (***p* < 0.01), but there was a significant increase in QC at 29°C (****p* < 0.001). **B**, Representative electrophysiological traces. Scale bars for EPSPs (and mEPSPs) are 5 mV (1 mV) and 50 ms (1000 ms). **C**, Cumulative frequency distribution comparing mEPSP values for the 25°C versus 29°C conditions. **D**, Box-and-whisker plots of mEPSP amplitude for the same genotypes. The 29°C condition showed a significantly diminished mEPSP distribution profile compared to 25°C (****p* < 0.001, Mann-Whitney test).

an; + denotes mean) and whiskers spanning 1st–99th percentiles, and individual extreme data points <1st or >99th percentile are plotted. See Table 2 for summary detail.

Results

Homeostatic potentiation using a dominant-negative glutamate receptor subunit

A prior study described a transgene encoding a dominant-negative *GluRIIA* subunit, *UAS-GluRIIA^{M614R}* (herein termed *GluRIIA^{M/R}* or dominant-negative; DiAntonio et al. 1999). The *GluRIIA* M614R amino acid substitution resides in the ion conduction pore of the *GluRIIA* subunit, and it cripples channel function (DiAntonio et al. 1999). Transgenic expression of *UAS-GluRIIA^{M/R}* in muscles renders a strong homeostatic challenge (markedly diminished quantal size) and an equally strong compensatory response (increase in quantal content). The prior report demonstrated that evoked amplitudes remain normal as a result of this compensation, presently termed presynaptic homeostatic potentiation (PHP; DiAntonio et al. 1999).

We acquired the dominant-negative transgenic line to test homeostatic reversibility. First, we replicated the published experiments, raising fruit fly larvae at temperatures

compatible with the TARGET system that we planned to use to test reversibility (McGuire et al. 2003). We tested 25°C (a common culturing temperature) and 29°C (a temperature at which the *GAL80^{TS}* protein ceases to inhibit *GAL4*). We drove *UAS-GluRIIA^{M/R}* expression with *MHC-Gal4*, which turns on in first-instar larval muscles (Schuster et al. 1996a, b). We recorded from NMJs of WT, *GAL4* driver control, and dominant-negative wandering third instar larvae.

For animals reared at 25°C, WT NMJ electrophysiology was robust and consistent with values canonically reported for WT at this synapse (Fig. 1A, C, D; Table 1 for raw electrophysiological data). For heterozygous *MHC-Gal4/+* driver control NMJs (“*MHC-Gal4*” on figures), we noted a small decrease in quantal size compared to WT (Figs. 1A, C, D). This quantal size decrease was consistent across the entire distribution of the spontaneous miniature excitatory postsynaptic potential (mEPSP) sample (Figs. 2A, B). Driver controls had a fully offsetting increase in QC, keeping evoked potentials robust (Figs. 1A, C; Table 1).

Muscle-specific expression of the *UAS-GluRIIA^{M/R}* dominant-negative transgene at 25°C caused a stark diminishment of quantal size and frequency compared to controls, evident from a small average mEPSP amplitude

Table 1. Raw electrophysiological data

Genotype	Condition	mEPSP noise		mEPSP/noise ratio	mEPSP frequency		EPSP (mV)	QC	I _R (MΩ)	RMP (mV)	n	Figure
		mEPSP (mV)	(μV)		(Hz)							
<i>w¹¹¹⁸ (WT)</i>	25°C	0.85 ± 0.04	16.5 ± 1.8	57.3 ± 5.7	3.5 ± 0.3	32.0 ± 1.2	38.5 ± 1.7	6.4 ± 0.6	-64.6 ± 1.1	13	1, 2	
<i>w¹¹¹⁸; MHC-Gal4/+</i>	25°C	0.65 ± 0.03	23.3 ± 1.2	28.2 ± 1.3	4.3 ± 0.5	33.6 ± 1.8	52.1 ± 1.8	4.8 ± 0.2	-66.1 ± 1.2	13	1, 2	
<i>UAS-GluRIIA^{M614R/+}; MHC-Gal4/+</i>	25°C	0.44 ± 0.02	13.8 ± 0.5	32.2 ± 1.7	0.6 ± 0.1	35.0 ± 1.8	80.3 ± 4.1	5.8 ± 0.5	-69.1 ± 1.2	11	1, 2	
<i>w¹¹¹⁸</i>	29°C	0.72 ± 0.03	16.7 ± 0.7	43.6 ± 2.2	1.8 ± 0.2	32.9 ± 1.2	46.4 ± 2.2	6.2 ± 0.5	-64.4 ± 0.9	14	1, 2	
<i>w¹¹¹⁸; MHC-Gal4/+</i>	29°C	0.52 ± 0.02	21.8 ± 0.7	24.1 ± 1.0	2.4 ± 0.1	31.7 ± 1.3	61.2 ± 2.4	5.3 ± 0.4	-66.5 ± 1.0	12	1, 2	
<i>UAS-GluRIIA^{M614R/+}; MHC-Gal4/+</i>	29°C	0.35 ± 0.02	13.8 ± 0.9	26.4 ± 2.3	0.2 ± 0.0	23.3 ± 1.2	68.9 ± 5.7	5.2 ± 0.2	-65.0 ± 1.1	10	1, 2	
<i>UAS-GluRIIA^{M614R/+}; MHC-Gal4/Gal80^{TS}</i>	Early third instar; 25°C	1.27 ± 0.1	26.6 ± 3.1	53.4 ± 7.3	2.0 ± 0.3	33.2 ± 2.1	27.4 ± 2.4	9.5 ± 0.8	-64.7 ± 2.0	10	3	
<i>UAS-GluRIIA^{M614R/+}; MHC-Gal4/Gal80^{TS}</i>	Early third instar; 29°C	0.60 ± 0.05	18.7 ± 1.9	32.8 ± 1.2	0.4 ± 0.1	25.1 ± 1.4	43.1 ± 2.6	13.6 ± 0.9	-63.0 ± 0.8	10	3	
<i>UAS-GluRIIA^{M614R/+}; MHC-Gal4/Gal80^{TS}</i>	21°C	0.83 ± 0.03			5.1 ± 0.5	33.3 ± 1.9	40.7 ± 2.4	5.6 ± 0.4	-66.3 ± 0.8	14	4, 5	
<i>UAS-GluRIIA^{M614R/+}; MHC-Gal4/Gal80^{TS}</i>	29°C	0.42 ± 0.02			0.4 ± 0.1	25.6 ± 2.1	62.5 ± 4.8	6.0 ± 0.3	-66.8 ± 1.1	15	4, 5	
<i>UAS-GluRIIA^{M614R/+}; MHC-Gal4/Gal80^{TS}</i>	1-d recovery at 21°C	0.39 ± 0.02			0.6 ± 0.1	24.1 ± 1.4	63.1 ± 5.0	5.3 ± 0.3	-66.0 ± 1.1	9	4, 5	
<i>UAS-GluRIIA^{M614R/+}; MHC-Gal4/Gal80^{TS}</i>	2-d recovery at 21°C	0.69 ± 0.02			3.4 ± 0.3	37.8 ± 1.2	55.4 ± 1.9	5.3 ± 0.3	-67.7 ± 0.7	10	4, 5	
<i>UAS-GluRIIA^{M614R/+}; MHC-Gal4/Gal80^{TS}</i>	3-d recovery at 21°C	0.80 ± 0.04			5.6 ± 0.4	35.3 ± 1.5	44.7 ± 1.7	5.5 ± 0.2	-68.4 ± 0.9	11	4, 5	
<i>UAS-GluRIIA^{M614R/+}; BG57-Gal4/Gal80^{TS}</i>	25°C	0.79 ± 0.04			2.4 ± 0.7	31.1 ± 1.6	39.5 ± 5.9	5.3 ± 0.4	-68.4 ± 1.1	13	6	
<i>UAS-GluRIIA^{M614R/+}; BG57-Gal4/Gal80^{TS}</i>	28.5°C	0.62 ± 0.05			0.6 ± 0.1	31.5 ± 1.3	53.6 ± 3.6	7.2 ± 0.4	-67.0 ± 1.3	13	6	
<i>UAS-GluRIIA^{M614R/+}; BG57-Gal4/Gal80^{TS}</i>	2-d recovery at 25°C	0.79 ± 0.03			1.4 ± 0.2	31.3 ± 1.4	39.9 ± 1.8	6.3 ± 0.3	-66.7 ± 1.1	14	6	
<i>w¹¹¹⁸</i>	30°C	0.78 ± 0.04			2.4 ± 0.2	33.1 ± 1.4	42.9 ± 1.9	6.8 ± 0.3	-66.2 ± 0.8	15	7	
<i>w¹¹¹⁸; GluRIIA^{SP16}</i>	30°C	0.32 ± 0.02			0.8 ± 0.1	21.9 ± 2.2	67.4 ± 6.8	6.0 ± 0.4	-63.0 ± 0.5	15	7	
<i>MHC-Gal4/+</i>	30°C	0.47 ± 0.02			1.1 ± 0.1	28.9 ± 0.6	64.3 ± 3.6	4.9 ± 0.2	-63.9 ± 0.9	15	7	
<i>UAS-GluRIIA^{M614R/+}; MHC-Gal4/+</i>	30°C	0.33 ± 0.01			0.2 ± 0.0	15.4 ± 1.1	47.0 ± 2.8	5.3 ± 0.2	-64.4 ± 0.9	13	7	
<i>w¹¹¹⁸; BG57-Gal4/+</i>	30°C	0.51 ± 0.03			0.6 ± 0.1	31.3 ± 1.4	63.9 ± 4.5	6.6 ± 0.3	-70.2 ± 1.4	12	7	
<i>UAS-GluRIIA^{M614R/+}; BG57-Gal4/+</i>	30°C	0.35 ± 0.03			0.8 ± 0.7	13.5 ± 1.3	39.1 ± 3.4	6.1 ± 0.5	-65.5 ± 1.6	9	7	
<i>w¹¹¹⁸</i>	31°C	0.71 ± 0.03			2.4 ± 0.2	36.9 ± 1.6	53.6 ± 3.0	2.0 ± 0.2	-68.1 ± 1.5	14	7	
<i>w¹¹¹⁸; GluRIIA^{SP16}</i>	31°C	0.36 ± 0.02			1.1 ± 0.2	25.8 ± 1.5	74.4 ± 5.4	4.2 ± 0.9	-66.6 ± 1.3	13	7	
<i>w¹¹¹⁸</i>	32°C	0.47 ± 0.01			2.4 ± 1.1	30.7 ± 1.9	64.8 ± 4.1	2.0 ± 0.4	-63.7 ± 0.9	13	7	
<i>w¹¹¹⁸; GluRIIA^{SP16}</i>	32°C	0.37 ± 0.03			1.4 ± 0.9	21.0 ± 2.2	56.1 ± 4.4	5.6 ± 0.3	-65.0 ± 0.8	10	7	

Full genotypes and rearing conditions for electrophysiological data presented in the study. Average values ± SEM are presented for each parameter; n, number of NMJs recorded. Values include mEPSP amplitude, noise, amplitude to noise ratio, and frequency; EPSP amplitude; quantal content (QC); muscle input resistance (I_R); and resting membrane potential (RMP).

and decreased mEPSP amplitudes across the entire distribution (Figs. 1A, C, and 2A, B; Table 1). Despite decreased quantal size, there was no diminishment in the average evoked excitatory postsynaptic potential (EPSP) amplitude for dominant-negative NMJs (Figs. 1A, C, D; Table 1)—again, because of a fully offsetting homeostatic increase in QC (Figs. 1A, C; Table 1). In sum, our recordings at 25°C agreed with the prior finding for the dominant-negative transgene (DiAntonio et al. 1999): full PHP.

For animals raised at 29°C, we garnered similar results as at 25°C, noting a few differences. At 29°C, WT NMJs had slightly smaller mEPSP quantal amplitude and frequency than 25°C WT NMJs (Fig. 1A–D; Table 1). This finding was consistent with a prior report measuring NMJ physiology at elevated temperatures (Ueda and Wu, 2015). WT EPSP amplitudes and QC at 29°C were nevertheless robust, similar to the values garnered at 25°C (Fig. 1A–D; Table 1). *MHC-Gal4/+* driver controls at 29°C showed slightly diminished average mEPSP amplitudes, a diminishment that persisted across the entire distribution of events (Figs. 1B, C, and 2C, D). *MHC-Gal4/+* driver

controls at 29°C maintained normal evoked potentials because of homeostatically increased QC (Fig. 1B–D).

By contrast, *UAS-GluRIIA^{M/R}*-expressing NMJs from 29°C showed a profound decrease in mEPSP size, a partially compensatory increase in QC compared to WT, and markedly reduced quantal frequency compared to WT (Figs. 1B, C, and 2C, D). Although QC was significantly increased in dominant-negative NMJs compared to WT, it did not increase enough to bring average dominant-negative EPSP amplitudes at 29°C fully back to WT or *MHC-Gal4/+* control levels (Fig. 1B–D).

The diminished mEPSP frequency for dominant-negative-expressing NMJs (Fig. 1C) is an interesting phenotype; it mirrors numerous cases at the *Drosophila* NMJ in which there is greatly diminished glutamate receptor subunit expression or function (Featherstone et al. 2005; Daniels et al. 2006; Kim et al. 2012, 2015; Brusich et al. 2015; Ramos et al. 2015). Given the very low observed mEPSP frequencies for dominant-negative NMJs, one potential concern was a severe underestimation of QC in these recordings due to unobserved mEPSP events that could have been lost in the noise of the recordings. In

Table 2. Statistical analysis

Data structure	Type of test or value reported	Confidence intervals
Normal distribution	Student's <i>t</i> test (Figs. 3, 7, 8)	* <i>p</i> < 0.05, ** <i>p</i> < 0.01, *** <i>p</i> < 0.001
Normal distribution	One-way ANOVA with Tukey's <i>post hoc</i> (Figs. 1, 2, 4, 6, 7, 8)	* <i>p</i> < 0.05, ** <i>p</i> < 0.01, *** <i>p</i> < 0.001
Cumulative distribution	Kruskal-Wallis test (Fig. 2: three data sets)	*** <i>p</i> < 0.001
Cumulative distribution	Mann-Whitney test (Fig. 3: two data sets)	*** <i>p</i> < 0.001
Nonlinear best-fit curve	R ² (Fig. 5)	Not applicable

theory, such lost events could confound analyses of homeostatic compensation. We calculated the average noise for mEPSP recordings from every genotype, as well as an mEPSP size/mEPSP noise ratio (Table 1). Noise varied slightly from genotype to genotype, but it was vanishingly small for each one (~0.02 mV/mEPSP for each; Table 1). This small noise yielded very large mEPSP/noise ratios for all genotypes (Table 1). Those ratios did vary because of different average quantal sizes between the genotypes; as a result, the ratio was a little smaller for dominant-negative NMJs than for WT controls (Table 1). Importantly, however, dominant-negative *GluRIIA^{M/R}*-expressing NMJs showed similar values by these noise measures at 25°C versus 29°C (Table 1). This indicated that recording noise was not a factor in determining full versus partial homeostatic compensation between the 25°C and 29°C conditions.

Early third instar larvae express homeostatic plasticity

Our initial experiments showed that it is possible to observe increases in QC for *UAS-GluRIIA^{M/R}*-expressing animals compared to WT, when raising flies at either 25°C or 29°C. We sought to test homeostatic reversibility. The TARGET system augments GAL4/*UAS* expression, adding a ubiquitously expressed *Tubulin_β-Gal80^{TS}* GAL4 inhibitor transgene (McGuire et al. 2003). We added this *GAL80^{TS}* expression feature to the *MHC-Gal4* >> *UAS-GluRIIA^{M/R}* genetic background. The temperature sensitivity of the *GAL80^{TS}* protein permits tight control over when GAL4-responsive transgenes are expressed (McGuire et al. 2003). We predicted that the dominant-negative transgene should be repressed by *GAL80^{TS}* at low temperatures; conversely, *UAS-GluRIIA^{M/R}* should be actively expressed when *GAL80^{TS}* is inactive (~29°C or higher; McGuire et al. 2003). To study the reversibility of PHP, animals could be reared at high temperature and then swapped to a lower temperature at an appropriate developmental time point.

An ideal temperature swap point would be late enough to detect PHP but early enough to allow recovery time after cessation of the dominant-negative *UAS-GluRIIA^{M/R}* expression. We crossed *UAS-GluRIIA^{M/R}*; *Tub_β-Gal80^{TS}* × *MHC-Gal4* stocks. Mated animals were transferred to 25°C or 29°C for egg laying and subsequent larval development. We selected early third instar progeny for electrophysiological recording. At temperature ranges of 25°C–29°C, early third instar larvae develop roughly 48–60 h after egg-laying. We staged these small animals unambiguously by examining their posterior spiracles for an orange-colored tip.

For animals raised entirely at 25°C, early third instar NMJ mEPSP size was large—significantly larger than one would observe for third instar larvae (Fig. 3A, B; Table 1; compare with Fig. 1). This was expected because small muscles have a significantly greater input resistance and enhanced quantal size (Lnenicka and Mellon, 1983a, b; Davis and Bezprozvanny, 2001; Table 1). Nevertheless, early third instar larval NMJs raised at 25°C showed normal evoked amplitudes, consistent with a stable level of

evoked muscle excitation throughout development (Fig. 3A, B; Table 1; compare with Fig. 1).

We expected that genotypically equivalent early third instars raised entirely at 29°C would express the dominant-negative transgene. NMJs from these 29°C animals showed sharply reduced average mEPSP amplitude and frequency compared to their stage- and size-matched counterparts raised at 25°C (Fig. 3A, B; Table 1), and this mEPSP amplitude decrease persisted throughout the distribution of events (Fig. 3C, D). There was a robust increase in quantal content at 29°C, resulting in EPSP amplitudes that were nearly normal, but not quite at the same level as at 25°C. Therefore, as with the earlier experiments, PHP for dominant-negative early third instar NMJs raised exclusively at 29°C was present, but not full (Fig. 3A, B; Table 1). Again, as a quality-check control, absolute mEPSP noise levels were small for both conditions (Table 1), and the mEPSP size/mEPSP noise ratios were similar to values obtained for the prior experiment (Table 1).

Partial homeostatic potentiation is reversible

At 29°C, PHP was not full, but QC increases versus controls were robust, still making it possible to test homeostatic reversibility. We generated additional *MHC-Gal4* >> *UAS-GluRIIA^{M/R}* larvae with the *Tub_β-GAL80^{TS}* transgene. For reversibility experiments, we chose 21°C as a permissive *GAL80^{TS}* shift temperature because 21°C permitted multiple electrophysiological time point measurements over a long recovery window (Fig. 4A).

Control (no PHP) animals raised entirely at 21°C took ~120 h after egg laying to reach the wandering third instar stage, whereas control (PHP) animals raised entirely at 29°C took ~96 h to reach the same stage (Fig. 4A). A 1-d recovery condition was used, exposing animals to the *UAS-GluRIIA^{M/R}* challenge for ~72 h (29°C) and allowing them to recover at 21°C for 1 d before recording. We also tested 2- and 3-d recovery conditions, rearing larvae at 29°C for ~49–50 h and then swapping them to 21°C until they reached wandering third instar stage. Because of the length of the egg lays and small variations in developmental time, some animals reached the wandering third instar recording stage after ~2 d at 21°C, and others took closer to 3 d (Fig. 4A).

Control *MHC-Gal4* >> *UAS-GluRIIA^{M/R}* larvae with ubiquitously expressed *Tub_β-Gal80^{TS}* and raised at 21°C showed neurotransmission indistinguishable from WT control animals reared at 25°C (compare Figs. 1 and 4; Table 1). By contrast, genetically identical control animals raised at 29°C throughout life showed electrophysiological phenotypes similar to dominant-negative *MHC-Gal4* >> *UAS-GluRIIA^{M/R}* animals raised at 29°C (compare Figs. 1 and 4; Table 1). Compared to counterparts raised at 21°C, animals raised at 29°C showed reduced mEPSP frequency, reduced mEPSP size, slightly below-normal EPSP amplitudes, and increased QC, indicating robust PHP (Fig. 4B, C; Table 1).

Recovery conditions showed physiologic signatures that corresponded with how much time was spent at 21°C. Compared to the 29°C condition, the 1-d 21°C

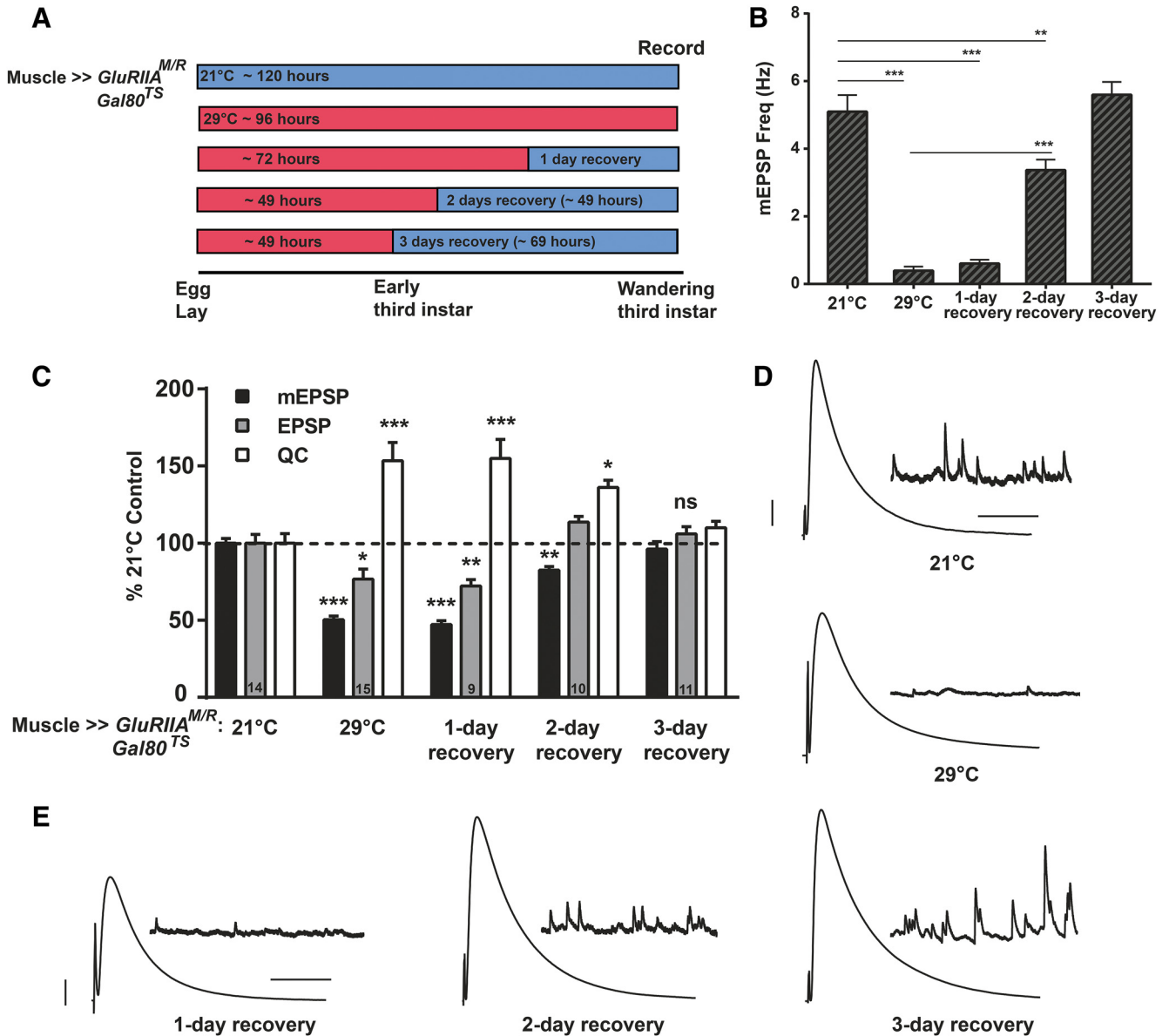


Figure 4. Presynaptic homeostatic potentiation is reversible. **A**, Diagram of a temperature swap paradigm. Mated animals laid eggs for a small window of 6–8 h. One set of larvae was reared entirely at 21° from egg laying to electrophysiological recording. A second set was raised entirely at 29°. To test for reversibility of homeostatic potentiation, additional sets were reared initially at 29°C and then swapped to 21°C. Animals were allowed to recover for 1, 2, or 3 d before recording. **B**, Expression of the dominant-negative transgene throughout life (29°C) caused a dramatic decrease in mEPSP frequency ($***p < 0.001$, one-way ANOVA with Tukey's *post hoc*). Frequency remained low after 1 d of recovery at 21°C, compared to baseline 21°C controls, but by 2 d of recovery, the frequency was significantly increased compared to 29°C ($***p < 0.001$), but still decreased compared to 21°C controls ($**p < 0.01$). By 3 d of recovery, mEPSP frequency was no different from animals raised entirely at 21°C. **C**, Normalized electrophysiological data for mEPSP amplitude, EPSP amplitude, and QC for the NMJs of animals raised as described in **A**. Longer recovery periods yielded electrophysiology that closely approximated the control 21°C rearing condition (all statistics: $*p < 0.05$, $**p < 0.01$, $***p < 0.001$ compared to 21°C control by one-way ANOVA with Tukey's *post hoc*). **D**, Representative electrophysiological traces for 21°C and 29°C. **E**, Traces for the three recovery conditions. Scale bars for EPSPs (and mEPSPs) are 5 mV (1 mV) and 50 ms (1000 ms) for both **D** and **E**.

recovery condition showed no significant changes in physiologic properties and no reversal of PHP (Fig. 4B–E). By contrast, the 2-d recovery condition showed intermediate physiology. Compared to constant exposure to 21°C, the 2-d recovery condition still had diminished mEPSP amplitude and frequency, but not nearly as diminished as con-

stant exposure to 29°C (Fig. 4B–E). Interestingly, the 2-d recovery EPSP amplitudes revealed fully restored levels of excitation, due to an offsetting QC level (Fig. 4C–E). The 3-d recovery condition showed electrophysiology that was not significantly different from the constant 21°C condition (Fig. 4B–E), indicating a full reversal of PHP.

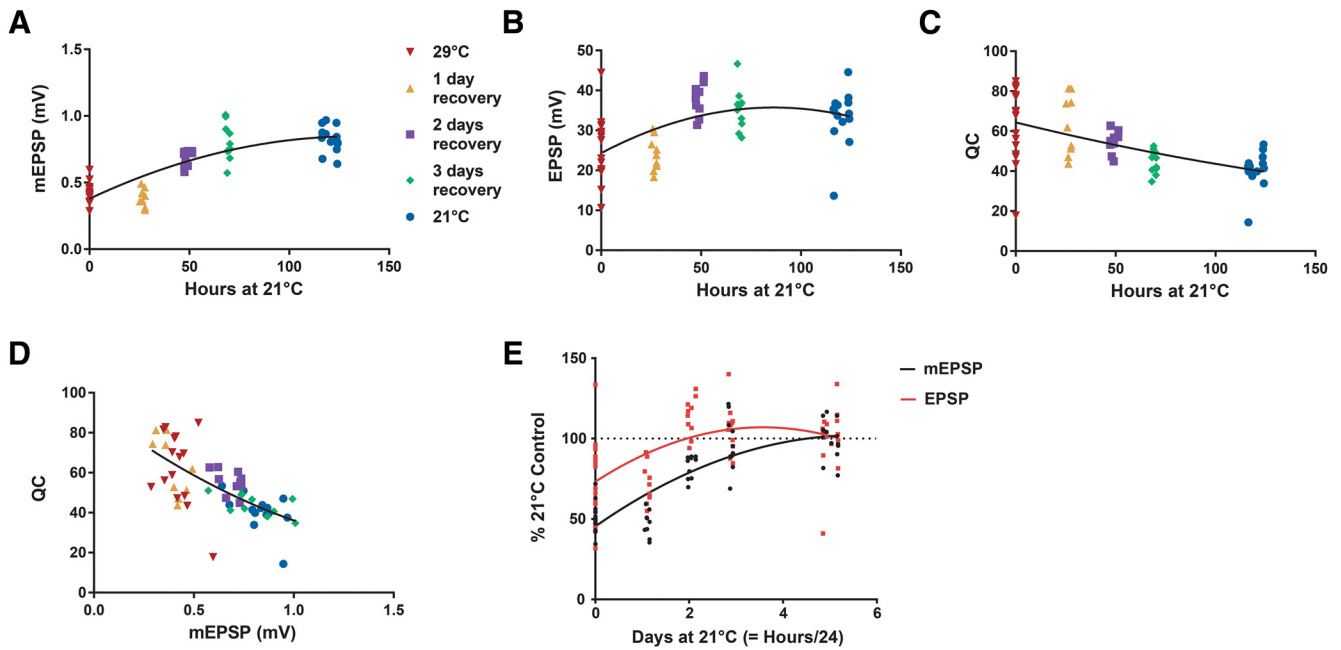


Figure 5. Strong correlations between recovery time and classic homeostatic parameters. Electrophysiological parameter data plotted from the reversibility experiments detailed in Fig. 4. Animals reared for “0 hours” at 21°C are the 29°C condition; animals in the 21°C condition were reared at that temperature for ~120 h. Each data point is time-locked to the times of the relevant egg-laying period and the recording. **A**, mEPSP amplitude plotted as a function of hours raised at 21°C. The data show a strong positive correlation between the two parameters ($R^2 = 0.71$; nonlinear fit as a quadratic equation). **B**, EPSP amplitude plotted as a function of hours raised at 21°C. The data show a positive correlation between the two values ($R^2 = 0.28$; nonlinear fit as a quadratic equation). **C**, QC plotted as a function of hours raised at 21°C. The data show a negative correlation between the two values ($R^2 = 0.34$; nonlinear fit as a quadratic equation). **D**, Plots of QC versus mEPSP amplitude for each recording. Consistent with prior reports examining PHP at the NMJ, there was a negative correlation between the two values ($R^2 = 0.47$; nonlinear fit as a quadratic equation). **E**, A comparison of quadratic fits for the mEPSP recovery curve ($y = -1.835x^2 + 20.38x + 45.41$) versus EPSP recovery curve ($y = -2.648x^2 + 18.93x + 73.18$). Both parameters are plotted as a percentage of the 21°C control values, as a function of days (= hours/24) reared at 21°C.

We further analyzed the aggregate data from the reversibility experiment. We wished to analyze reversal parameters related to recovery time. We plotted mEPSP (Fig. 5A), EPSP (Fig. 5B) and QC (Fig. 5C) values versus the number of hours animals spent at the recovery temperature, with a specific recovery time value for each NMJ, time-locked to the egg laying period and the recording time after recovery/development at 21°C. Each plot showed hallmarks of PHP reversal: mEPSP and EPSP amplitudes positively correlated with time at 21°C (Fig. 5A, B), and QC values inversely correlated with time at 21°C (Fig. 5C). Consistent with the observation that PHP was present (but not full) at 29°C, individual data points from NMJs of animals raised entirely at 29°C showed a wide variability of QC values (Fig. 5C). Prior studies of homeostatic plasticity at the *Drosophila* NMJ have shown that by analyzing hundreds of individual recording values, QC inversely scales with quantal size across genotypes, and as a result, evoked excitation levels remain stable (Frank et al. 2006; Davis and Müller, 2015; Gaviño et al. 2015). For our temperature swap experiments—this time conducting a comparison within a single genotype—this also proved to be the case (Fig. 5D). Finally, we checked whether there was a leading component to the recovery, testing whether mEPSP and EPSP values recovered at similar or different rates. We coplotted each parameter’s

recovery curve relative to the 21°C control values and fitted the nonlinear curves with quadratic functions. Both parameters appear to recover at similar rates, with the EPSP values reaching the 21°C baseline level first (Fig. 5E).

Full homeostatic potentiation is also reversible

Homeostatic potentiation was robust, yet partial, at the 29°C condition. We hoped to test a condition that was both compatible with full PHP and the reversibility assay. We attempted a new temperature swap, changing parameters. We reasoned that by making the environmental challenge to the NMJ less harsh—by using a lower temperature, putting forth a less severe level glutamate receptor loss, or both—we would be able to generate an ideal full PHP reversibility test condition. For one change, we lowered the restrictive GAL80^{TS}-impairing temperature from 29°C to 28.5°C. Other studies using the TARGET system in *Drosophila* have reported that 28.5°C is somewhat effective at impairing GAL80^{TS} function (Staley and Irvine, 2010; Corrigan et al. 2014; Redhai et al. 2016). Second, we replaced the *MHC-Gal4* muscle driver with the *BG57-Gal4* muscle driver (Budnik et al. 1996). Finally, we tried 25°C as the permissive condition.

We generated new sets of larvae for this swap experiment: *BG57-Gal4* >> *UAS-GluRIIA^{M/R}* larvae with the *TubP-Gal80^{TS}* transgene. As expected, animals raised at 25°C

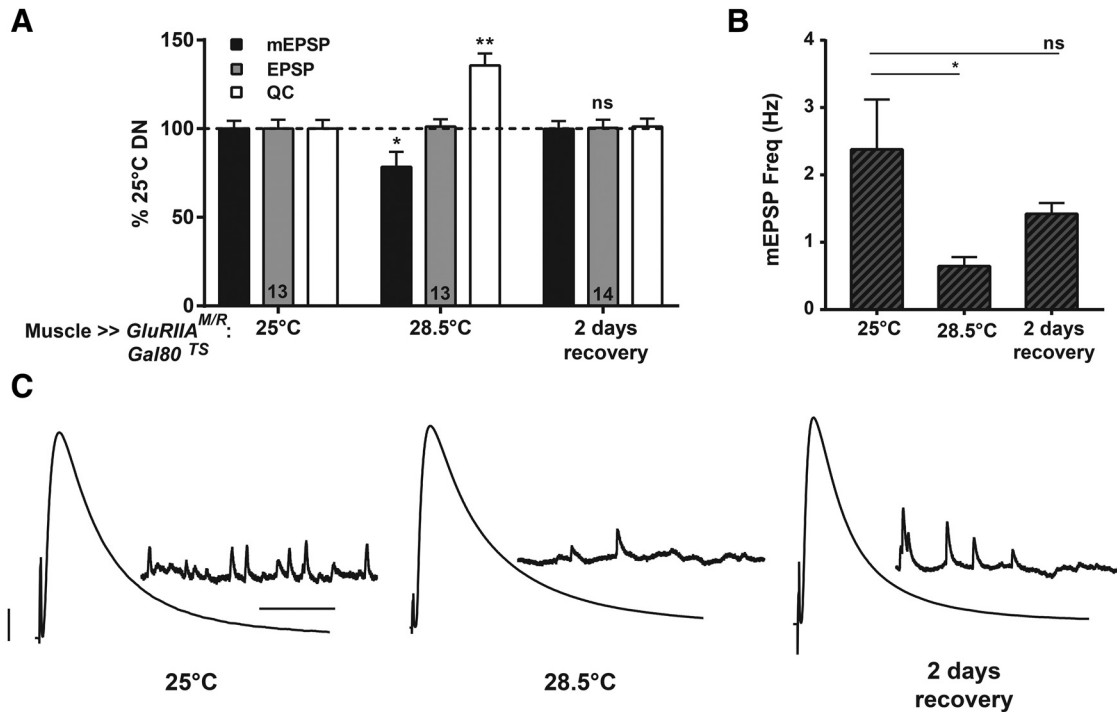


Figure 6. Full homeostatic compensation is reversible. **A**, Dominant-negative animals with the *Gal80^{TS}* transgene raised at 28.5°C showed a significant decrease in mEPSP amplitude (**p* < 0.05, compared to 25°C condition; one-way ANOVA with Tukey’s *post hoc*), accompanied by a fully offsetting increase in QC (***p* < 0.01). Reversibility of homeostatic potentiation was demonstrated by initially rearing *w; GluRIIA^{M/R/+}; BG57-Gal4/Gal80^{TS}* animals at 28.5°C for 2 d and swapping them to 25°C for 2 d. mEPSP amplitude, EPSP amplitude, and QC returned to control (25°C throughout life) levels. EPSP amplitudes were virtually identical across all of the conditions. **B**, Dominant-negative animals raised at 28.5°C throughout life showed a significant decrease in mEPSP frequency (**p* < 0.05, one-way ANOVA with Tukey’s *post hoc*). In contrast, the mEPSP frequency in animals after 2 d of recovery was not significantly different from that of the animals reared at 25°C. **C**, Representative electrophysiological traces. Scale bars for EPSPs (and mEPSPs) are 5 mV (1 mV) and 50 ms (1000 ms).

throughout life (*GAL80^{TS}* on) developed NMJs with electrophysiological properties similar to other control conditions already reported (Fig. 6A, C; Table 1). Also as expected, animals raised at 28.5°C throughout life (*GAL80^{TS}* impaired) had significantly diminished NMJ mEPSP amplitudes (Fig. 6A; Table 1). Of note, the 28.5°C NMJs had markedly diminished mEPSP frequency (Fig. 6B), which is an indication of successful expression of the dominant-negative *GluRIIA^{M/R}* transgene (Fig. 1). NMJs from those 28.5°C animals also showed completely normal EPSP amplitudes because of a full, offsetting homeostatic increase in QC (Fig. 6A, C; Table 1). Finally, animals raised at 28.5°C until early third instar and then swapped to 25°C for the final 2 d of larval development showed NMJ electrophysiology indistinguishable from that of animals raised at 25°C throughout life, indicating a complete reversal of PHP (Fig. 6).

Homeostatic potentiation induced by glutamate receptor function loss is impaired at high temperatures

UAS-GluRIIA^{M/R} transgene-induced homeostatic potentiation was robust, yet partial, at the 29°C condition. We wondered whether PHP might specifically be impaired at the NMJ when flies are raised at high temperatures. An alternative idea is that a functional limit of the homeostatic signaling system could be due to a dual combination of

factors challenging synapse function, such as high temperature combined with glutamate receptor function loss.

To test this idea further, we drove the dominant-negative transgene in the muscle, setting up crosses to generate both *MHC-Gal4 >> UAS-GluRIIA^{M/R}* and *BG57-Gal4 >> UAS-GluRIIA^{M/R}* animals, as well as driver-specific controls. For the driver controls, quantal size was somewhat diminished at 30°C (Fig. 7A–D; Table 1). This was consistent with the idea that quantal size is generally diminished at very high temperatures (Ueda and Wu, 2015), although taken together with our prior results (Fig. 1), it also seemed likely that simply driving *GAL4* protein in the muscle can cause this phenotype. Despite diminished quantal size, evoked EPSP amplitudes were still robust for 30°C driver controls because of homeostatic increases in QC (Fig. 7A–D; Table 1). For the dominant-negative NMJs, there was a significant reduction in mEPSP size beyond what was measured for the driver controls. Moreover, evoked amplitudes were weak, diminished significantly versus driver controls because of no significant increase in QC versus WT controls (Fig. 7A–D; Table 1). These data indicated that signaling processes that maintain PHP in response to the dominant-negative transgene may break down at high temperatures.

We were uncertain whether this high-temperature failure in PHP was due to the expression levels of the

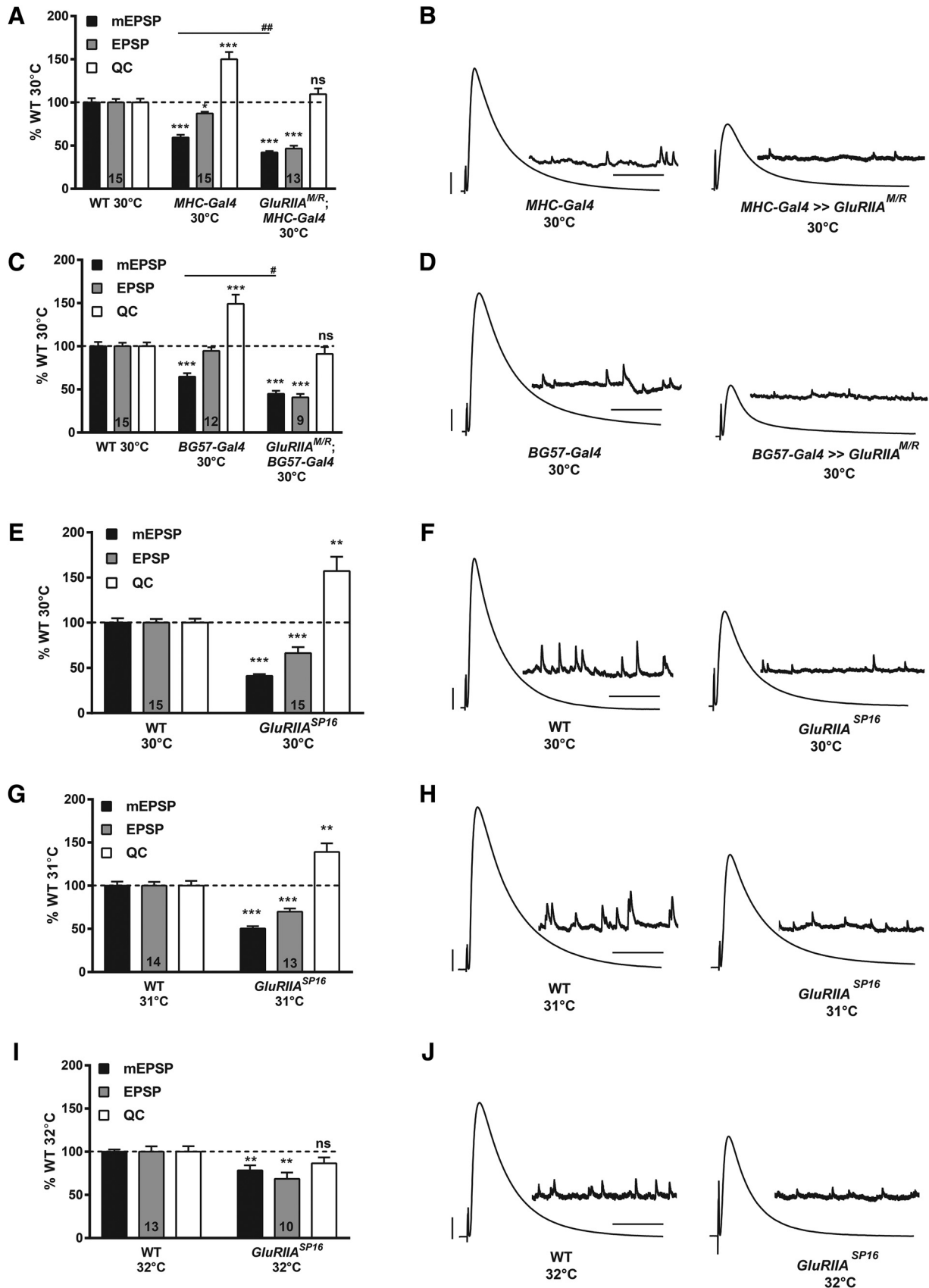


Figure 7. Presynaptic homeostatic potentiation can be impaired at high temperatures. **A**, WT (w^{1118}), driver controls ($w;; MHC-Gal4/+$), and dominant-negative NMJs ($w;; UAS-GluRIIA^{M/R}/+; MHC-Gal4/+$) were compared at 30°C. For driver controls, the mEPSP amplitude

continued

was significantly decreased compared to WT ($***p < 0.001$, one-way ANOVA with Tukey's *post hoc*), but the EPSP amplitude was only slightly smaller than normal ($*p < 0.05$ versus WT) because of a homeostatic increase in QC ($***p < 0.001$ versus WT). For dominant-negative animals, the mEPSP amplitude was markedly decreased ($***p < 0.001$ versus WT; $\#p < 0.01$ versus driver controls, one-way ANOVA with Tukey's *post hoc*). A dramatic decrease in EPSP amplitude for the dominant-negative NMJs also occurred ($***p < 0.001$ versus WT) because there was no significant change in QC ($p = 0.58$ versus WT), indicating a block of PHP. **B**, Representative electrophysiological traces. Scale bars for EPSPs (and mEPSPs) are 5 mV (1 mV) and 50 ms (1000 ms). **C**, WT, driver controls (w ; $BG57-Gal4/+$), and dominant-negative animals (w ; $UAS-GluRIIA^{MIR}/+; BG57-Gal4/+$) were compared at 30°C. For driver controls, the mEPSP amplitude was significantly decreased compared to WT ($***p < 0.001$, one-way ANOVA with Tukey's *post hoc*), but the EPSP was normal because of a homeostatic increase in QC ($***p < 0.001$ versus WT). In contrast, for dominant-negative animals, the mEPSP amplitude was markedly decreased ($***p < 0.001$ versus WT; $\#p < 0.01$ versus driver controls, one-way ANOVA with Tukey's *post hoc*). A dramatic decrease in EPSP amplitude for the dominant-negative NMJs also occurred ($***p < 0.001$ versus WT) because there was no significant change in QC ($p = 0.71$), indicating a block of PHP. **D**, Representative electrophysiological traces. Scale bars as in **B**. **E**, $GluRIIA^{SP16}$ animals and WT controls were raised at 30°C. mEPSPs were significantly decreased for $GluRIIA$ mutants ($***p < 0.001$, Student's *t* test). EPSP values were also decreased ($***p < 0.001$) but not to the same magnitude as mEPSP amplitudes because the QC was significantly increased ($**p < 0.01$). **F**, Representative electrophysiological traces. Scale bars as in **B**. **G**, $GluRIIA^{SP16}$ animals and WT controls were raised at 31°C. mEPSP and EPSP amplitude were both significantly decreased in $GluRIIA^{SP16}$ animals ($***p < 0.001$, Student's *t* test) and QC was increased ($**p < 0.01$). **H**, Representative electrophysiological traces. Scale bars as in **B**. **I**, The same genotypes were raised at 32°C. $GluRIIA^{SP16}$ animals showed a decrease in mEPSP and EPSP amplitude ($**p < 0.01$, Student's *t* test), and they failed to show increase in QC ($p = 0.17$). **J**, Representative electrophysiological traces. Scale bars as in **B**.

dominant-negative glutamate receptor subunit at 30°C, the high temperature, or a combination of both. High temperature alone seemed unlikely, because the 30°C driver controls also had diminished quantal size accompanied by robust PHP. Glutamate receptor function loss alone also seemed unlikely, because quantal size for the dominant-negative NMJs was not starkly diminished at 30°C compared to earlier experiments run at 25°C and 29°C (Fig. 1; Table 1).

To extend our inquiry, we examined an additional homeostatic challenge to NMJ function. We raised WT and $GluRIIA^{SP16}$ null deletion flies (Petersen et al. 1997) at 30°C, 31°C, and 32°C. WT NMJs showed relatively normal physiology at 30° and 31°C (Fig. 7E–H; Table 1). Interestingly, NMJs from $GluRIIA^{SP16}$ deletion animals raised at 30° and 31°C showed significant PHP, with reduced mEPSP amplitudes and robust increases in QC compared to WT (Fig. 7A, B; Table 1). However, we noted that $GluRIIA^{SP16}$ EPSP amplitudes were reduced compared to WT, meaning that the PHP was only partial (Table 1). These $GluRIIA^{SP16}$ QC data (Fig. 7E, G) and the 30°C muscle-driver control QC data (Fig. 7A, C) argue against the notion that high temperature alone completely impairs PHP. Temperature could still be a contributing factor.

We next raised WT and $GluRIIA^{SP16}$ null animals at 32°C. This extreme temperature was suboptimal for animal health. WT animals, while able to reach the third instar stage, had poor muscle health, as measured by low input resistance and low mEPSP amplitude compared to conditions of normal rearing temperatures (Table 1). Nevertheless, 32°C WT NMJs had evoked events that were nearly normal in size (Fig. 7I, J; Table 1). Homozygous $GluRIIA^{SP16}$ larvae that survived to the wandering third instar stage at 32°C were rare. For the 32°C $GluRIIA^{SP16}$ homozygotes that did survive, the NMJs showed a further decrease in mEPSP amplitude and no PHP expression (Fig. 7I, J; Table 1). Taken together, the electrophysiological data are consistent with the idea that a dual chal-

lenge—glutamate receptor function loss plus extreme high temperature—abolishes PHP.

Dual-challenged NMJs show diminished growth at high temperatures

We asked whether synaptic growth defects might correlate with PHP deficits when raising glutamate receptor-compromised animals at high temperatures. We took larvae raised in a subset of the high temperature conditions described (Fig. 7) and immunostained NMJs with anti-Synapsin (Syn, presynaptic vesicles) and anti-Discs Large (Dlg, postsynaptic density) antibodies to assess NMJ development by immunofluorescence. We quantified synaptic bouton elaboration. For dominant-negative glutamate receptor expression under $MHC-Gal4$ control, there was a sharp decrease in NMJ growth at 30°C compared to the 29°C condition (Fig. 8A–C). By contrast, $BG57-Gal4$ -driven dominant-negative expression elicited sharply diminished growth at both 29°C and 30°C (Fig. 8A, B).

For WT and $GluRIIA^{SP16}$, we collected NMJ growth data over a range of temperatures: 21°, 29°, and 30°C. At 21°C, growth was similar between the two genotypes (Fig. 8D, E). At 29°C, an impairment of NMJ growth in $GluRIIA^{SP16}$ nulls was apparent, whereas WT NMJ growth was still relatively normal (Fig. 8D, E). At 30°C, both WT and $GluRIIA^{SP16}$ nulls showed diminished overall growth (Fig. 8D–F), with $GluRIIA^{SP16}$ growth numerically (but not statistically) diminished. At 30°C for these genotypes, the anti-Syn staining had a tendency to appear disorganized, spreading out over a larger area in the presynaptic bouton (Fig. 8F). Collectively, these data are consistent with the idea that at high temperatures under conditions of glutamate receptor loss, PHP failure correlates with NMJ growth and development defects. It is uncertain whether these growth parameters are causally related to the limit in homeostatic signaling.

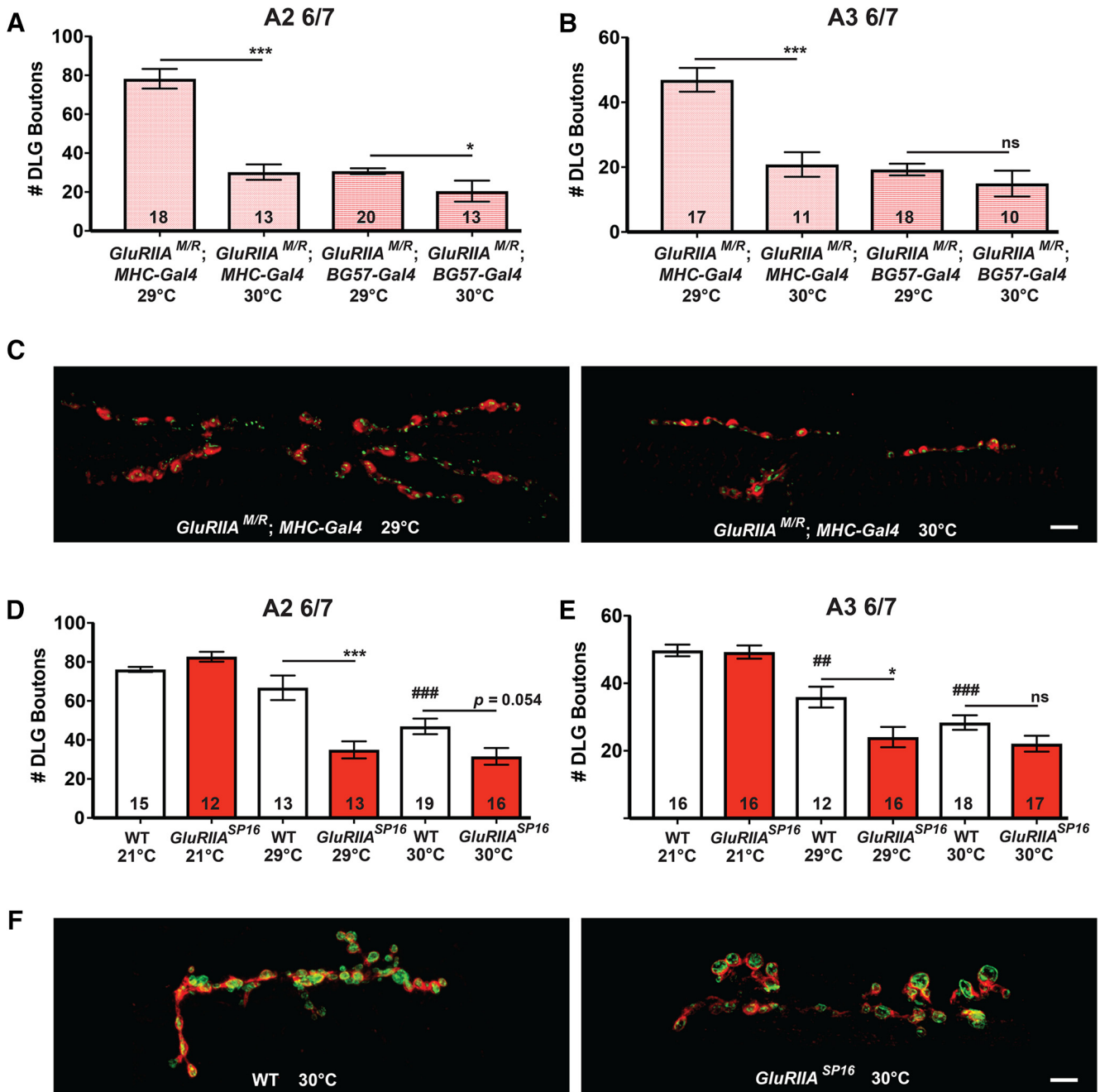


Figure 8. NMJ undergrowth correlates with glutamate receptor function loss plus high temperature. **A**, *w; UAS-GluRIIA^{M/R}/+; MHC-Gal4/+* and *w; UAS-GluRIIA^{M/R}/+; BG57-Gal4/+* animals were raised at 29°C or 30°C and costained with anti-DLG (red) and anti-Synapsin antibodies (green) to visualize synaptic boutons. Boutons were counted based on postsynaptic DLG staining and double checked for presynaptic Synapsin. At abdominal segment A2 muscle 6/7, *w; UAS-GluRIIA^{M/R}/+; MHC-Gal4/+* animals raised at 30°C showed a significant decrease in bouton number compared to genetically identical counterparts raised at 29°C ($***p < 0.001$, Student's *t* test). *w; UAS-GluRIIA^{M/R}/+; BG57-Gal4/+* animals raised at 30°C showed only a slight decrease in bouton number compared to counterparts at 29°C ($*p < 0.05$), although in this case, the 29°C NMJs already showed stunted growth. **B**, Boutons were also quantified at synapse A3 6/7. *w; UAS-GluRIIA^{M/R}/+; MHC-Gal4/+* animals raised at 30°C showed a significant decrease in bouton number compared to counterparts raised at 29°C ($***p < 0.001$). There was no significant difference between 29°C and 30°C for *w; UAS-GluRIIA^{M/R}/+; BG57-Gal4/+* animals; again, both conditions for this genotype showed severely stunted NMJ elaboration. **C**, Representative NMJ images of synapse A2 6/7 for *w; GluRIIA^{M/R}/+; MHC-Gal4/+* animals raised at 29°C and 30°C. Scale bar, 10 μ m. **D**, WT and *GluRIIA^{SP16}* animals were raised at 21°C, 29°C, or 30°C and stained with anti-DLG (red) and anti-Synapsin (green). At 29°C, *GluRIIA^{SP16}* animals showed a significant decrease in bouton number compared to 29°C WT controls ($***p < 0.001$, one-way ANOVA with Tukey's *post hoc*). Additionally, WT NMJs raised at 30°C showed decreased growth compared to WT counterparts raised at 21°C ($###p < 0.001$). **E**, DLG boutons were quantified at abdominal segment 3 for the same genotypes. *GluRIIA^{SP16}* NMJs at 29°C showed a decrease in bouton number compared to WT at the same temperature ($*p < 0.05$). Additionally,

continued

WT NMJs raised at 29°C ($##p < 0.01$) and 30°C ($###p < 0.001$) showed decreased growth compared to the 21°C condition. **F**, Representative images of synapse A2 6/7 WT and *GluRIIA*^{SP16} NMJs at 30°C, showing few boutons and a disorganized anti-Synapsin pattern. Scale bar, 10 μ m.

Discussion

For the *Drosophila* NMJ, homeostatic potentiation is a robust and sensitive process. One assumption supported by all available data is that the larval NMJ is capable of modulating its vesicle release at any time point during development, in accordance with the presence or absence of a homeostatic challenge to synapse function. Rapid, acute induction of homeostatic signaling has been demonstrated at the *Drosophila* NMJ by application of PhTox to impair the glutamate receptors (Frank et al. 2006), but the reversibility of this particular modulation (or any other modulation at the *Drosophila* NMJ) had not been studied. More generally, it is not clear what happens in metazoan nervous systems when strong perturbations that induce homeostatic signaling are introduced for long periods of developmental time and then later removed.

We present evidence that PHP at the *Drosophila* neuromuscular synapse is a reversible process. In doing so, we confirm prior findings showing that there is a tight inverse relationship between quantal amplitude and QC at the NMJ (Fig. 5). We complement those findings with the results of temperature shift experiments. We find that PHP is measurable at an early stage of larval development (Fig. 3) and can be erased over a matter of days (Figs. 4–6). Interestingly, at high temperatures, PHP induced by impairing glutamate receptor function either fails or falls short of full compensation (Figs. 1, 3, 4, 7). This failure appears to correlate with impaired NMJ growth in the same animals (Fig. 8).

Why is reversibility slow after dominant-negative *GluRIIA*^{M/R} removal?

There was a robust expression of PHP for NMJs of *MHC-Gal4* \gg *UAS-GluRIIA*^{M/R} larvae with the *TubP-Gal80^{TS}* transgene raised at 29°C for 48 h after egg-laying (Fig. 3). Once the expression of the dominant-negative *UAS-GluRIIA*^{M/R} transgene was halted, this expression of PHP was erased over a slow 48- to 72-h period (Fig. 4).

If PHP is a readily reversible homeostatic process, why is there a days-long time lag to reverse it? Our data likely reflect a constraint of the dominant-negative *GluRIIA*^{M/R} experimental perturbation, rather than the NMJ's capacity to respond quickly to the changed environment. In a prior study, researchers expressed functional, tagged *GluRIIA* transgenic subunits at the NMJ and performed fluorescence recovery after photobleaching (FRAP) experiments (Rasse et al. 2005). Those experiments demonstrated that receptor turnover rates at the *Drosophila* NMJ are extremely slow: it appears that once postsynaptic densities (PSDs) reach a critical size, *GluRIIA* subunits are stably incorporated (Rasse et al. 2005). For our study, this likely means that the temperature downshifts in the reversibility experiments (Figs. 4 and 6) represented an opportunity for the NMJ to incorporate endogenous WT *GluRIIA* into a significant number of new PSDs while it continued to grow

(Rasse et al. 2005; Schmid et al. 2006, 2008). Given sufficient growth, the endogenously expressed *GluRIIA* would gradually overcome the previously incorporated dominant-negative *GluRIIA*^{M/R} subunits. This would restore electrophysiological parameters to normal levels, which is consistent with our data.

Reversibility of rapid and sustained forms of homeostatic plasticity

The majority of recent studies about synaptic homeostasis at the *Drosophila* NMJ have emphasized that presynaptic adjustments to neurotransmitter release properties must occur within minutes of drug-induced (PhTox) postsynaptic receptor inhibition to induce a rapid and offsetting response to PhTox challenge. Some important parameters uncovered through these studies include regulation of presynaptic Ca^{2+} influx (Frank et al. 2006, 2009; Müller and Davis, 2012; Younger et al. 2013; Wang et al. 2014, 2016a); regulation of the size of the readily releasable pool (RRP) of presynaptic vesicles (Weyhersmüller et al. 2011; Harris et al. 2015; Müller et al. 2015, 2012; Wang et al. 2016a); control of presynaptic SNARE-mediated fusion events (Dickman and Davis, 2009; Müller et al. 2011; Dickman et al. 2012); control of neuronal excitability (Bergquist et al. 2010; Younger et al. 2013; Parrish et al. 2014; Orr et al. 2017b); and recently, implication of endoplasmic reticulum calcium-sensing activities (Genç et al. 2017; Kikuma et al. 2017); presynaptic glutamate receptor activity (Kiragasi et al. 2017); and finally, identification of a retrograde, trans-synaptic signaling system governed by the Semaphorin 2b ligand and the Plexin B receptor (Orr et al. 2017a).

For almost all of the cases in which a mutation or an experimental condition blocks the short-term induction of homeostatic signaling, the same perturbation has also been shown to block its long-term maintenance. Interestingly, however, the converse is not true. Additional studies have shown that the long-term consolidation (or expression) of homeostatic signaling at the NMJ can be genetically uncoupled from its induction. Select molecules seem to be dedicated to a long-term maintenance program that involves protein translation and signaling processes in both the neuron and the muscle (Frank et al. 2009; Marie et al. 2010; Penney et al. 2012; Brusich et al. 2015; Kauwe et al. 2016; Spring et al. 2016). Recent data suggest that such long-term processes may take 6 h or more to take full effect (Kauwe et al. 2016).

As more molecular details about HSP are elucidated, it will be interesting to test whether the rapid induction and sustained consolidation of PHP can be reversed by similar or separate mechanisms, and what the time courses of those reversal mechanisms are. At the mouse NMJ, reversibility was recently demonstrated pharmacologically. D-Tubocurarine was applied at a subblocking concentration to impair postsynaptic acetylcholine receptors. Within

seconds of drug application, QC increased—and then within seconds of drug washout, it decreased again (Wang et al. 2016b). Follow-up experiments suggested that those rapid, dynamic changes in PHP dynamics at the mouse NMJ were mediated by a calcium-dependent increase in the size of the RRP of presynaptic vesicles (Wang et al. 2016b). Because there seem to be several similarities between the mouse NMJ and the *Drosophila* NMJ (Frank, 2014; Davis and Müller, 2015), it is possible that PHP at the insect NMJ can also be rapidly reversed.

It is instructive to consider mammalian synaptic preparations and study how homeostatic forms of synaptic plasticity are turned on and off. Groundbreaking work on cultured excitatory vertebrate synapses showed that in response to activity deprivation (or promotion), synapses employ scaling mechanisms by adding (or subtracting) AMPA-type glutamate receptors to counteract the perturbation (O'Brien et al. 1998; Turrigiano et al. 1998). Bidirectional scaling suggested that reversible mechanisms likely dictate homeostatic scaling processes. Complementary studies testing scaling reversibility have borne out this prediction (Rutherford et al. 1997; Swanwick et al. 2006; Wang et al. 2011). Additionally, evidence for reversible forms of homeostatic scaling have been found in rodent sensory systems, such as auditory synapses after hearing deprivation (and restoration to reverse; Whiting et al. 2009) and in the visual cortex after light deprivation (and restoration to reverse; Goel and Lee, 2007). Collectively, the vertebrate and invertebrate studies support the notion that reversible fine-tuning is an efficient strategy used to stabilize activities in metazoan nervous systems. One advantage offered by the *Drosophila* system is a genetic toolkit to uncover possible reversibility factors.

Partial or failed homeostatic signaling at high temperatures

Are there environmental limitations for homeostatic potentiation at the *Drosophila* NMJ? Clearly there are. Our data suggest that a combination of high temperature (30°C–32°C) plus impaired glutamate receptor function can severely limit the NMJ's ability to compensate for reduced neurotransmitter sensitivity. High temperature alone does not seem to be a severe enough restriction to impair PHP, because *Gal4* driver controls at 30°C have somewhat reduced quantal size, but a fully (or nearly fully) offsetting increase in QC (Fig. 7A–D). Likewise, reduced glutamate receptor function alone does not appear to be a sufficient barrier to impair PHP. For example, quantal size is severely diminished when the dominant negative *UAS-GluRIIA^{M/R}* transgene is expressed at 25°C, but PHP is nevertheless intact (Fig. 1A).

It is not clear what the molecular or anatomic basis of this limit on PHP is. We do know that it is not an issue of NMJ excitation at high temperatures, because evoked neurotransmission for WT (or driver control) NMJs remains remarkably robust over a range of temperatures, including 30°C (Table 1). Nor does it seem to be an elimination of PHP in general, because PHP was still present in the case of *GluRIIA^{SP16}* animals raised at 30°C (Fig. 6; Table 1), revealing a distinction between the null

GluRIIA condition and the dominant-negative *GluRIIA* condition. The limitation seems to be on homeostatic signaling that supports PHP at high temperatures in the face of the dominant-negative transgene expression.

Temperature effects on neurophysiology are well documented. Recent work in crustaceans demonstrates that robust and reliable circuits such as the neurons driving the rhythmicity stomatogastric nervous system can fail under extreme temperature challenges (Tang et al. 2012; Rinberg et al. 2013; Marder et al. 2015). For the *Drosophila* NMJ, prior studies of larval development documented a significant enhancement of synaptic arborization when larvae were raised at higher temperatures (Sigrist et al. 2003; Zhong and Wu, 2004). Additional studies have shown that NMJ growth plasticity can be additionally affected by mutations that affect neuronal excitability (Budnik et al. 1990; Zhong et al. 1992; Lee and Wu, 2010). Given the backdrop of these data, it is not unreasonable to hypothesize that the tolerable limits of synaptic activity challenge could be different at different temperatures.

For our experiments, 29°C–32°C represents a potential failure zone for homeostatic potentiation at the *Drosophila* NMJ. We must note that our data suggest that the coping capacity of the NMJ is dependent on genotype. WT NMJs cope at all temperatures. By contrast, for dominant-negative *GluRIIA*-expressing NMJs, 29°C is a point at which PHP becomes partial (Figs. 1 and 2), and 30°C is a point at which it fails (Fig. 6). For *GluRIIA^{SP16}* subunit deletion NMJs, there is robust, but partial PHP at 30°C (Fig. 7), not unlike the compensation seen for the dominant-negatives at 29°C. *GluRIIA^{SP16}* NMJs fail to execute PHP only when temperature is pushed to an extreme range, such as 32°C. Why do these differences persist? It is not clear. The answer could relate to the well-documented temperature-induced alterations in NMJ growth, or alternatively, a limited availability of synaptic factors that are needed to cope with a double challenge of high temperature and particular impairment of glutamate receptor function. Future molecular and physiologic work will be needed to unravel those possibilities in the contexts of different genetic backgrounds and culturing conditions.

References

- Bergquist S, Dickman DK, Davis GW (2010) A hierarchy of cell intrinsic and target-derived homeostatic signaling. *Neuron* 66:220–234. [CrossRef](#) [Medline](#)
- Brusich DJ, Spring AM, Frank CA (2015) A single-cross, RNA interference-based genetic tool for examining the long-term maintenance of homeostatic plasticity. *Front Cell Neurosci* 9:107 [CrossRef](#)
- Budnik V, Koh YH, Guan B, Hartmann B, Hough C, Woods D, Gorczyca M (1996) Regulation of synapse structure and function by the *Drosophila* tumor suppressor gene *dlg*. *Neuron* 17:627–640. [Medline](#)
- Budnik V, Zhong Y, Wu CF (1990) Morphological plasticity of motor axons in *Drosophila* mutants with altered excitability. *J Neurosci* 10:3754–3768.
- Burrone J, O'Byrne M, Murthy VN (2002) Multiple forms of synaptic plasticity triggered by selective suppression of activity in individual neurons. *Nature* 420:414–418. [CrossRef](#)
- Corrigan L, Redhai S, Leiblich A, Fan SJ, Perera SM, Patel R, Gandy C, Wainwright SM, Morris JF, Hamdy F, et al. (2014) BMP-

- regulated exosomes from *Drosophila* male reproductive glands reprogram female behavior. *J Cell Biol* 206:671–688. [CrossRef](#)
- Cull-Candy SG, Miledi R, Trautmann A, Uchitel OD (1980) On the release of transmitter at normal, myasthenia gravis and myasthenic syndrome affected human end-plates. *J Physiol* 299:621–638. [CrossRef](#)
- Daniels RW, Collins CA, Chen K, Gelfand MV, Featherstone DE, DiAntonio A (2006) A single vesicular glutamate transporter is sufficient to fill a synaptic vesicle. *Neuron* 49:11–16. [CrossRef](#)
- Daniels RW, Collins CA, Gelfand MV, Dant J, Brooks ES, Krantz DE, DiAntonio A (2004) Increased expression of the *Drosophila* vesicular glutamate transporter leads to excess glutamate release and a compensatory decrease in quantal content. *J Neurosci* 24:10466–10474. [CrossRef](#)
- Davis GW, Bezprozvanny I (2001) Maintaining the stability of neural function: a homeostatic hypothesis. *Annu Rev Physiol* 63:847–869. [CrossRef](#) [Medline](#)
- Davis GW, DiAntonio A, Petersen SA, Goodman CS (1998) Postsynaptic PKA controls quantal size and reveals a retrograde signal that regulates presynaptic transmitter release in *Drosophila*. *Neuron* 20:305–315. [CrossRef](#)
- Davis GW, Goodman CS (1998) Synapse-specific control of synaptic efficacy at the terminals of a single neuron. *Nature* 392:82–86. [CrossRef](#) [Medline](#)
- Davis GW, Müller M (2015) Homeostatic control of presynaptic neurotransmitter release. *Annu Rev Physiol* 77:251–270. [CrossRef](#)
- DiAntonio A, Petersen SA, Heckmann M, Goodman CS (1999) Glutamate receptor expression regulates quantal size and quantal content at the *Drosophila* neuromuscular junction. *J Neurosci* 19:3023–3032.
- Dickman DK, Davis GW (2009) The schizophrenia susceptibility gene dysbindin controls synaptic homeostasis. *Science* 326:1127–1130. [CrossRef](#)
- Dickman DK, Tong A, Davis GW (2012) Snapin is critical for presynaptic homeostatic plasticity. *J Neurosci* 32:8716–8724. [CrossRef](#) [Medline](#)
- Featherstone DE, Rushton E, Rohrbough J, Liebl F, Karr J, Sheng Q, Rodesch CK, Broadie K (2005) An essential *Drosophila* glutamate receptor subunit that functions in both central neuropil and neuromuscular junction. *J Neurosci* 25:3199–3208.
- Frank CA (2014) Homeostatic plasticity at the *Drosophila* neuromuscular junction. *Neuropharmacology* 78:63–74. [CrossRef](#)
- Frank CA, Kennedy MJ, Goold CP, Marek KW, Davis GW (2006) Mechanisms underlying the rapid induction and sustained expression of synaptic homeostasis. *Neuron* 52:663–677. [CrossRef](#)
- Frank CA, Pielage J, Davis GW (2009) A presynaptic homeostatic signaling system composed of the Eph receptor, ephexin, Cdc42, and CaV2.1 calcium channels. *Neuron* 61:556–569. [CrossRef](#)
- Gaviño MA, Ford KJ, Archila S, Davis GW (2015) Homeostatic synaptic depression is achieved through a regulated decrease in presynaptic calcium channel abundance. *eLife* 4:e05473. [CrossRef](#)
- Genç Ö, Dickman DK, Ma W, Tong A, Fetter RD, Davis GW (2017) MCTP is an ER-resident calcium sensor that stabilizes synaptic transmission and homeostatic plasticity. *eLife* 6:e22904. [CrossRef](#)
- Goel A, Lee HK (2007) Persistence of experience-induced homeostatic synaptic plasticity through adulthood in superficial layers of mouse visual cortex. *J Neurosci* 27:6692–6700. [CrossRef](#)
- Harris N, Braiser DJ, Dickman DK, Fetter RD, Tong A, Davis GW (2015) The innate immune receptor PGRP-LC controls presynaptic homeostatic plasticity. *Neuron* 88:1157–1164. [CrossRef](#)
- Hazelrigg T, Levis R, Rubin GM (1984) Transformation of white locus DNA in *Drosophila*: dosage compensation, zeste interaction, and position effects. *Cell* 36:469–481. [CrossRef](#)
- Kauwe G, Tsurudome K, Penney J, Mori M, Gray L, Calderon MR, Elazouzi F, Chicoine N, Sonenberg N, Haghghi AP (2016) Acute fasting regulates retrograde synaptic enhancement through a 4E-BP-dependent mechanism. *Neuron* 92:1204–1212. [CrossRef](#)
- Kikuma K, Li X, Kim D, Sutter D, Dickman DK (2017) Extended synaptotagmin localizes to presynaptic ER and promotes neurotransmission and synaptic growth in *Drosophila*. *Genetics* 207:993–1006.
- Kim YJ, Bao H, Bonanno L, Zhang B, Serpe M (2012) *Drosophila* Neto is essential for clustering glutamate receptors at the neuromuscular junction. *Genes Dev* 26:974–987. [CrossRef](#)
- Kim YJ, Igiesuorobo O, Ramos CI, Bao H, Zhang B, Serpe M (2015) Prodomain removal enables neto to stabilize glutamate receptors at the *Drosophila* neuromuscular junction. *PLoS Genetics* 11:e1004988. [CrossRef](#)
- Kiragasi B, Wondolowski J, Li Y, Dickman DK (2017) A presynaptic glutamate receptor subunit confers robustness to neurotransmission and homeostatic potentiation. *Cell Reports* 19:2694–2706. [CrossRef](#)
- Lee J, Wu CF (2010) Orchestration of stepwise synaptic growth by K⁺ and Ca²⁺ channels in *Drosophila*. *J Neurosci* 30:15821–15833. [CrossRef](#) [Medline](#)
- Lnenicka GA, Mellon D Jr. (1983a) Changes in electrical properties and quantal current during growth of identified muscle fibres in the crayfish. *J Physiol* 345:261–284.
- Lnenicka GA, Mellon D Jr. (1983b) Transmitter release during normal and altered growth of identified muscle fibres in the crayfish. *J Physiol* 345:285–296.
- Marder E, Bucher D (2007) Understanding circuit dynamics using the stomatogastric nervous system of lobsters and crabs. *Annu Rev Physiol* 69:291–316. [CrossRef](#)
- Marder E, Goaillard JM (2006) Variability, compensation and homeostasis in neuron and network function. *Nat Rev Neurosci* 7:563–574. [CrossRef](#) [Medline](#)
- Marder E, Haddad SA, Goeritz ML, Rosenbaum P, Kispersky T (2015) How can motor systems retain performance over a wide temperature range? Lessons from the crustacean stomatogastric nervous system. *J Comp Physiol A Neuroethol Sens Neural Behav Physiol Neuroethol Sens Neural Behav Physiol* 201:851–856. [CrossRef](#)
- Marder E, Prinz AA (2002) Modeling stability in neuron and network function: the role of activity in homeostasis. *Bioessays* 24:1145–1154. [CrossRef](#) [Medline](#)
- Marie B, Pym E, Bergquist S, Davis GW (2010) Synaptic homeostasis is consolidated by the cell fate gene gooseberry, a *Drosophila* pax3/7 homolog. *J Neurosci* 30:8071–8082. [CrossRef](#) [Medline](#)
- McGuire SE, Le PT, Osborn AJ, Matsumoto K, Davis RL (2003) Spatiotemporal rescue of memory dysfunction in *Drosophila*. *Science* 302:1765–1768. [CrossRef](#) [Medline](#)
- Müller M, Davis GW (2012) Transsynaptic control of presynaptic Ca²⁺(+) influx achieves homeostatic potentiation of neurotransmitter release. *Curr Biol* 22:1102–1108. [CrossRef](#)
- Müller M, Genç Ö, Davis GW (2015) RIM-binding protein links synaptic homeostasis to the stabilization and replenishment of high release probability vesicles. *Neuron* 85:1056–1069. [CrossRef](#)
- Müller M, Liu KS, Sigrist SJ, Davis GW (2012) RIM controls homeostatic plasticity through modulation of the readily-releasable vesicle pool. *J Neurosci* 32:16574–16585. [CrossRef](#)
- Müller M, Pym EC, Tong A, Davis GW (2011) Rab3-GAP controls the progression of synaptic homeostasis at a late stage of vesicle release. *Neuron* 69:749–762. [CrossRef](#) [Medline](#)
- Murthy VN, Schikorski T, Stevens CF, Zhu Y (2001) Inactivity produces increases in neurotransmitter release and synapse size. *Neuron* 32:673–682. [Medline](#)
- O'Brien RJ, Kamboj S, Ehlers MD, Rosen KR, Fischbach GD, Huganir RL (1998) Activity-dependent modulation of synaptic AMPA receptor accumulation. *Neuron* 21:1067–1078.
- Orr BO, Fetter RD, Davis GW (2017a) Retrograde semaphorin-plexin signalling drives homeostatic synaptic plasticity. *Nature* 550:109–113.
- Orr BO, Gorczyca D, Younger MA, Jan LY, Jan YN, Davis GW (2017b) Composition and control of a Deg/ENaC channel during presynaptic homeostatic plasticity. *Cell Reports* 20:1855–1866.
- Parrish JZ, Kim CC, Tang L, Bergquist S, Wang T, Derisi JL, Jan LY, Jan YN, Davis GW (2014) Kruppel mediates the selective rebalancing of ion channel expression. *Neuron* 82:537–544. [CrossRef](#)

- Penney J, Tsurudome K, Liao EH, Elazzouzi F, Livingstone M, Gonzalez M, Sonenberg N, Haghghi AP (2012) TOR is required for the retrograde regulation of synaptic homeostasis at the *Drosophila* neuromuscular junction. *Neuron* 74:166–178. [CrossRef](#)
- Petersen SA, Fetter RD, Noordermeer JN, Goodman CS, DiAntonio A (1997) Genetic analysis of glutamate receptors in *Drosophila* reveals a retrograde signal regulating presynaptic transmitter release. *Neuron* 19:1237–1248. [CrossRef](#)
- Plomp JJ, Van Kempen GT, De Baets MB, Graus YM, Kuks JB, Molenaar PC (1995) Acetylcholine release in myasthenia gravis: regulation at single end-plate level. *Ann Neurol* 37:627–636. [CrossRef](#)
- Plomp JJ, van Kempen GT, Molenaar PC (1992) Adaptation of quantal content to decreased postsynaptic sensitivity at single endplates in alpha-bungarotoxin-treated rats. *J Physiol* 458:487–499. [CrossRef](#)
- Ramos CI, Igiesuorobo O, Wang Q, Serpe M (2015) Neto-mediated intracellular interactions shape postsynaptic composition at the *Drosophila* neuromuscular junction. *PLoS Genetics* 11:e1005191 [CrossRef](#)
- Rasse TM, Fouquet W, Schmid A, Kittel RJ, Mertel S, Sigrist CB, Schmidt M, Guzman A, Merino C, Qin G, et al . (2005) Glutamate receptor dynamics organizing synapse formation in vivo. *Nat Neurosci* 8:898–905. [CrossRef](#)
- Redhai S, Hellberg JE, Wainwright M, Perera SW, Castellanos F, Kroeger B, Gandy C, Leiblich A, Corrigan L, Hilton T, et al . (2016) Regulation of dense-core granule replenishment by autocrine BMP signalling in *Drosophila* secondary cells. *PLoS Genet* 12:e1006366. [CrossRef](#)
- Rinberg A, Taylor AL, Marder E (2013) The effects of temperature on the stability of a neuronal oscillator. *PLoS Comput Biol* 9:e1002857. [CrossRef](#) [Medline](#)
- Rongo C, Kaplan JM (1999) CaMKII regulates the density of central glutamatergic synapses in vivo. *Nature* 402:195–199. [CrossRef](#)
- Rutherford LC, DeWan A, Lauer HM, Turrigiano GG (1997) Brain-derived neurotrophic factor mediates the activity-dependent regulation of inhibition in neocortical cultures. *J Neurosci* 17:4527–4535.
- Schmid A, Hallermann S, Kittel RJ, Khorramshahi O, Frölich AM, Quentin C, Rasse TM, Mertel S, Heckmann M, Sigrist SJ (2008) Activity-dependent site-specific changes of glutamate receptor composition in vivo. *Nat Neurosci* 11:659–666. [CrossRef](#)
- Schmid A, Qin G, Wichmann C, Kittel RJ, Mertel S, Fouquet W, Schmidt M, Heckmann M, Sigrist SJ (2006) Non-NMDA-type glutamate receptors are essential for maturation but not for initial assembly of synapses at *Drosophila* neuromuscular junctions. *J Neurosci* 26:11267–11277. [CrossRef](#)
- Schuster CM, Davis GW, Fetter RD, Goodman CS (1996a) Genetic dissection of structural and functional components of synaptic plasticity. I. Fasciclin II controls synaptic stabilization and growth. *Neuron* 17:641–654.
- Schuster CM, Davis GW, Fetter RD, Goodman CS (1996b) Genetic dissection of structural and functional components of synaptic plasticity. II. Fasciclin II controls presynaptic structural plasticity. *Neuron* 17:655–667.
- Sigrist SJ, Reiff DF, Thiel PR, Steinert JR, Schuster CM (2003) Experience-dependent strengthening of *Drosophila* neuromuscular junctions. *J Neurosci* 23:6546–6556.
- Spring AM, Brusich DJ, Frank CA (2016) C-terminal Src kinase gates homeostatic synaptic plasticity and regulates fasciclin II expression at the *Drosophila* neuromuscular junction. *PLoS Genet* 12:e1005886. [CrossRef](#)
- Staley BK, Irvine KD (2010) Warts and Yorkie mediate intestinal regeneration by influencing stem cell proliferation. *Curr Biol* 20:1580–1587. [CrossRef](#) [Medline](#)
- Swanwick CC, Murthy NR, Kapur J (2006) Activity-dependent scaling of GABAergic synapse strength is regulated by brain-derived neurotrophic factor. *Mol Cell Neurosci* 31:481–492. [CrossRef](#)
- Tang LS, Taylor AL, Rinberg A, Marder E (2012) Robustness of a rhythmic circuit to short- and long-term temperature changes. *J Neurosci* 32:10075–10085. [CrossRef](#) [Medline](#)
- Thiagarajan TC, Lindskog M, Tsien RW (2005) Adaptation to synaptic inactivity in hippocampal neurons. *Neuron* 47:725–737. [CrossRef](#) [Medline](#)
- Turrigiano GG (2008) The self-tuning neuron: synaptic scaling of excitatory synapses. *Cell* 135:422–435. [CrossRef](#) [Medline](#)
- Turrigiano GG (2017) The dialectic of Hebb and homeostasis. *Philos Trans R Soc Lond B Biol Sci* 5:372. [CrossRef](#)
- Turrigiano GG, Leslie KR, Desai NS, Rutherford LC, Nelson SB (1998) Activity-dependent scaling of quantal amplitude in neocortical neurons. *Nature* 391:892–896. [CrossRef](#)
- Ueda A, Wu CF (2015) The role of cAMP in synaptic homeostasis in response to environmental temperature challenges and hyperexcitability mutations. *Front Cell Neurosci* 9:10. [CrossRef](#)
- Wang HL, Zhang Z, Hintze M, Chen L (2011) Decrease in calcium concentration triggers neuronal retinoic acid synthesis during homeostatic synaptic plasticity. *J Neurosci* 31:17764–17771. [CrossRef](#)
- Wang T, Hauswirth AG, Tong A, Dickman DK, Davis GW (2014) Endostatin is a trans-synaptic signal for homeostatic synaptic plasticity. *Neuron* 83:616–629. [CrossRef](#)
- Wang T, Jones RT, Whippen JM, Davis GW (2016a) alpha2delta-3 is required for rapid transsynaptic homeostatic signaling. *Cell Reports* 16:2875–2888.
- Wang X, Pinter MJ, Rich MM (2016b) Reversible recruitment of a homeostatic reserve pool of synaptic vesicles underlies rapid homeostatic plasticity of quantal content. *J Neurosci* 36:828–836.
- Wefelmeyer W, Puhl CJ, Burrone J (2016) Homeostatic plasticity of subcellular neuronal structures: from inputs to outputs. *Trends Neurosci* 39:656–667. [CrossRef](#)
- Weyhersmüller A, Hallermann S, Wagner N, Eilers J (2011) Rapid active zone remodeling during synaptic plasticity. *J Neurosci* 31:6041–6052. [CrossRef](#) [Medline](#)
- Whiting B, Moiseff A, Rubio ME (2009) Cochlear nucleus neurons redistribute synaptic AMPA and glycine receptors in response to monaural conductive hearing loss. *Neuroscience* 163:1264–1276. [CrossRef](#)
- Wierenga CJ, Ibata K, Turrigiano GG (2005) Postsynaptic expression of homeostatic plasticity at neocortical synapses. *J Neurosci* 25:2895–2905. [CrossRef](#) [Medline](#)
- Younger MA, Müller M, Tong A, Pym EC, Davis GW (2013) A presynaptic ENaC channel drives homeostatic plasticity. *Neuron* 79:1183–1196. [CrossRef](#) [Medline](#)
- Zhong Y, Budnik V, Wu CF (1992) Synaptic plasticity in *Drosophila* memory and hyperexcitable mutants: role of cAMP cascade. *J Neurosci* 12:644–651. [Medline](#)
- Zhong Y, Wu CF (2004) Neuronal activity and adenylyl cyclase in environment-dependent plasticity of axonal outgrowth in *Drosophila*. *J Neurosci* 24:1439–1445. [CrossRef](#)